Response to reviewers of wes-2016-21, "Wind turbine power production and annual energy production depend on atmospheric stability and turbulence" by C. M. St. Martin, J. K. Lundquist, A. Clifton, G. S. Poulos, and S. J. Schreck.

Reviewer #1:

This manuscript uses nacelle-based and upwind met tower measured data to calculate power curves (PC) and annual energy production for a specific wind turbine. This work thoroughly investigates the sensitivity of the PC and AEP to atmospheric parameters such as turbulence intensity (TI), Turbulence Kinetic Energy (TKE) and Bulk Richardson Number (RB) which would be of value to manufacturers in power performance testing. As indicated by the authors, the existing literature do not agree on the effects that these atmospheric parameters have on the PC and AEP.

Although the present work provides significant observations about the effect of TI, TKE and RB on power performance, it does not elaborate on the underlying physics of the obtained results. Also, this work does not provide any insights towards the factors that can contribute to the variability in the results reported in the existing literature.

We thank the reviewer for this assessment. We have added the following passage to a new Section 4.1.1 (Results – Underlying physics) to explain the underlying physics behind the results of this work:

> "The large variability reported in the literature (and herein) regarding power production can be understood by recognizing the interactions between a pitch-controlled turbine and the atmosphere: the operation of control algorithms changes with wind speed, with varying effects depending on the ambient turbulence.
>
> Sensitivity to atmospheric turbulence occurs at low wind speeds, near cut-in wind speed. In these conditions, the turbine generator speed (revolutions per minute, RPM) increases, as does the generator torque. As a result, the blades will often pitch backward, changing the angle of attack to generate more lift, and the power production ramps up. At low wind speeds and higher turbulence, the turbine can react to the higher variation in wind speed and can capitalize on the variation seen in the wind flow because of the additional lift resulting from the blade pitch, and the turbine produces more power. Conversely, at low wind speeds with lower turbulence, the variation in wind speed is lower, and so the turbine experiences more consistent wind than in highly turbulent conditions and therefore produces less power.
>
> At higher wind speeds, closer to or just below rated speed, control mechanisms seek to maintain rated generator speed, rather than continuing to

increase generator speed. The blades will pitch forward (or "feather"), allowing the power production to maintain rated power. This process effectively decreases the amount of lift when compared to lift generated by a non-feathered blade. At these wind speeds during periods of high TI, a turbine reacts to the high variation in wind speed with subtle changes in blade pitch. For example, if the turbine detects a drop in wind speed, the blades may pitch back to generate more lift, but then if the wind speed increases quickly after, the blades will pitch forward again. If the blade pitch cannot immediately respond to increases in wind speed, then power losses occur. At these higher wind speeds, lower turbulence enables consistent blade pitch to match atmospheric conditions, and so the turbine can capture more power.

It is also important to mention the strong connection between turbulence and shear: high shear will eventually erode turbulence (Wharton and Lundquist 2012a). Periods of high shear generally coincide with periods of low turbulence and vice versa. With low shear, the mean wind speed is more consistent over the height of the rotor disk. However, since we did not see significant differences in power curves for different shear regimes here, we cannot speculate further on this in this analysis. Finally, if veer occurs in the wind profile (as in Vanderwende and Lundquist 2012 and Dörenkamper et al. 2015), which usually occurs only in stable or low turbulence atmospheric conditions, that veer will generally undermine power production as the turbine blades are not oriented perpendicular to the flow at all vertical levels."

Specific comments:

Power curve measurements using hub height winds result in high uncertainties and are not a good representative of the energy contents of the flow. How does this known fact play role in the current study?

If the reviewer is referring to the use of nacelle-based wind measurements, then the reviewer brings up an important and relevant issue. We have added a short paragraph in Section 3.4 (Power curves) further explaining the issues resulting from the interference of the rotor disk on the ambient wind:

"The nacelle-mounted anemometer does not observe the ambient wind speed that the rotor disk experiences because the wind that flows through the rotor disk and along the nacelle during operation is modified by the blades and nacelle (Antoniou and Pedersen 1997; Smith et al. 2002; Frandsen et al. 2009; Zahle and Sørensen 2011). However, power curves calculated using nacelle wind speeds are shown here along with power curves calculated using upwind measurements in

order to compare the different methods. In many cases, operators calculate these nacelle-based power curves due to lack of other data."

References that have been added:

Antoniou, I., and Pedersen, T.F.: Nacelle Anemometry on a 1MW Wind Turbine, Risø National Laboratory, Roskilde, Denmark, 37 pp., 1997.

Frandsen, S., Sørensen, J.N., Mikkelsen, R., Pederesen, T.F., Antoniou, I., and Hansen, K.: The generics of wind turbine nacelle anemometry, Proceedings of European Wind Energy Conference, Marseille, France, 2009.

Smith, B., Link, H., Randall, G., and McCoy, T.: Applicability of Nacelle Anemometer Measurements for Use in Turbine Power Performance Tests, AWEA Windpower, Portland, OR, 2002.

Zahle, F., and Sørensen, N.N.: Characterization of the unsteady flow in the nacelle region of a modern wind turbine, Wind Energy, 13, 271-283, doi: 10.1002/we.418, 2011.

P5: Did you perform any data quality control on the 3D sonic measured values? If yes, what is the total number of data points remained for 3D sonic and why resulted in less number of data points for this instrument compared to the other met tower instruments?

Yes, data quality control filters presented in Section 3.1.2 (Analysis methods – Data quality control – Meteorological tower) were also applied to the sonic anemometers. In addition, several spikes in the sonics were filtered, which resulted in fewer data points in the analysis. The following sentence has been added to Section 3.1.2 describing the de-spiking methodology used:

> "Several spikes in wind speed occur in the raw sonic anemometer data. Therefore, a de-spiking filter is applied based on the change in wind speed from each data point to the next. Data points are removed if they are preceded and followed by changes exceeding the lowest 99 % of all changes. After filtering the spikes in the sonic anemometers as well as the previously discussed quality control procedure, the sonic anemometers provide wind speed and temperature about 90 % of the time at 15 m and about 60 % at 74 m during this study."

P8: It is not clear how the authors came up with a different classification for RB. This needs to be explained in more detail.

To expand upon the discussion in Section 3.5 (Atmospheric stability regimes), that R_B regimes were based on similar work performed at the NREL-NWTC (Aitken et al. 2014), we have added the following passage to the text in Section 3.5 to make the classification methodology more clear:

> "Similar to the approach used in Aitken et al. (2014), the R_B distribution is split roughly into thirds to allow for less overlap between stable and unstable regimes.

The uncertainty in R_B for these instruments over the measurement period is about 0.01, therefore the R_B classifications used are larger than the uncertainty."

P9: It appears that L values are calculated using 80m measurement data. Since at 80m only cup anemometers are installed, how is w' obtained?

The reviewer comments on an important detail that has been added to the text in Section 3.5 (Atmospheric stability regimes). The *L* values were calculated using sonic measurements at 15 m. The reviewer also asks about w'. The revised text more clearly states that sonic anemometer measurements are used to calculate *L*:

"*L* calculations are based on sonic anemometer measurements at 15 m and temperature measurements interpolated to 15 m to ensure *L* is calculated using measurements within the surface layer."

P12: Observations are made regarding the differences between nacelle power curves and tower curves and their dependency on the wind speed range (Lines266-276). However, no discussion is provided as to what are the possible explanations for such observations/ behavior.

We have expanded on the existing discussion to add the underlined text to Section 4.1 (Results – Power curves):

"Statistically-distinct wind speed bins in power curves calculated from nacelle winds tended to be similar to those in power curves calculated from tower winds near rated speed. At lower wind speeds, however, between about 5 and 9 m s^{-1}, many more statistically distinct differences emerged between nacelle power curves than between tower power curves, most notably in the power curves segregated by TI regimes. Turbine operations were especially variable in this region of rapid increase in power with wind speed. The turbine reacted directly to the conditions as measured by instruments on the turbine. The nacelle anemometer observes complex flows behind the rotor disk that are strongly influenced by ambient turbulence, leading to more statistically significant differences in the nacelle power curves for TI regimes."

P13: Authors have used power curves calculated using upwind tower data to obtain AEP. Given the variability observed between the tower data and the nacelle data, it would be interesting to look at the AEP values calculated using power curves obtained using nacelle measurements.

The authors agree and have calculated AEP based on the nacelle measurements as well. The results were added to Table 5 and are discussed in Section 4.2.

	No filter	TI filter	R_B filter
AEP using tower data	7,479.3	7,409.6	7,278.7
AEP using nacelle data	7,430.6	7,388.9	7,266.7

"AEP results in Table 5 also show that the AEP calculated using nacelle winds underestimates the AEP when compared with an AEP calculated using upwind tower measurements. This underestimation of the nacelle anemometer-calculated AEP is true for both the AEP calculated for the entire dataset as well as with each stability or turbulence filter and is likely because the nacelle anemometer underestimates the ambient wind speed due to flow interference of the rotor disk and nacelle."

P14: Given the lack of statistically significant impact of wind shear on the power curves and the AEP values provided in Table 5 for shear filter, one cannot make a conclusive statement about the effect of shear on AEP.

We have removed those AEP results in the revision.

P15: the authors suggest calculating different power curves for different conditions. Now the questions is with the practicality of this approach.

The reviewer brings up an interesting point of discussion, and the authors have added the following passage to Section 5 (Conclusions):

"As a small percent difference in AEP leads to a large deviation in cost for both operators and manufacturers, calculating different power curves for different atmospheric conditions may not only be a practical approach, but may lower the financial risks for both operators and manufacturers."

Technical corrections:

Fig 1: this figure is not providing the required information. I suggest that you replace this with a schematic drawing which marks and labels the turbine, the lidar and the met tower. Also include prevailing wind direction.

We have included a new, clearer Figure 1 that includes labels for each instrument as well as the prevailing wind direction.

Fig 6: "Grey line represents.." It should read "black line..."

We thank the reviewer for catching this error. We have made this change.

Fig 17: mark rated wind speed on the graphs

We have added a grey, dashed line marking rated speed on all figures showing the power curve.

The vertical axis on all distribution plots is not representing frequency but rather the number of points. This needs to be corrected.

We have replaced the number of points with relative frequency.

Reviewer #2:

This manuscript is trying to give the guidance of using a multi-criteria approach of evaluating power performance of a wind turbine. The concept of using of stability and turbulence filters in segregating power curves is not new, but the case study done in this manuscript and the associated evidence shown are of great value as a reference for the future work under this topic. The effort of collecting and quality controlling of the measured data from three sources: nacelle, tower and lidar are very noticeable. In the following years I hope I will continue my work in turbulent wind inflow study and would love to cite this paper when published and will try using numerical weather forecasting model/ large simulation model interacting with wind turbine models to reproduce the results found in this manuscript. I find the paper to be very well written.

We thank the reviewer for their kind comments.

There is just one general comment: This manuscript spreads out the observed relations between power curves/annual energy production (AEP) and turbulence intensity (TI)/ turbulence kinetic energy (TKE)/Bulk Richardson number(RB), however, the physics behind the phenomenons have not been discussed. For example, what are the authors' perspectives and explanations on the causes of "increased TI and TKE undermined power production at wind speeds near rated, but increased power production at lower wind speeds" ? The illustrative examples look appealing and it may be published if this lack of information is added.

We thank the reviewer for this motivation to address the underlying physics in more detail. We have added the following passage to a new Section 4.1.1 (Results – Underlying physics):

> "The large variability reported in the literature (and herein) regarding power production can be understood by recognizing the interactions between a pitch-controlled turbine and the atmosphere: the operation of control algorithms changes with wind speed, with varying effects depending on the ambient turbulence.
>
> Sensitivity to atmospheric turbulence occurs at low wind speeds, near cut-in wind speed. In these conditions, the turbine generator speed (revolutions per minute, RPM) increases, as does the generator torque. As a result, the blades will often pitch backward, changing the angle of attack to generate more lift, and the power production ramps up. At low wind speeds and higher turbulence, the turbine can react to the higher variation in wind speed and can capitalize on the variation seen in the wind flow because of the additional lift resulting from the blade pitch, and the turbine produces more power. Conversely, at low wind speeds with lower turbulence, the variation in wind speed is lower, and so the turbine experiences more consistent wind than in highly turbulent conditions and therefore produces less power.

At higher wind speeds, closer to or just below rated speed, control mechanisms seek to maintain rated generator speed, rather than continuing to increase generator speed. The blades will pitch forward (or "feather"), allowing the power production to maintain rated power. This process effectively decreases the amount of lift when compared to lift generated by a non-feathered blade. At these wind speeds during periods of high TI, a turbine reacts to the high variation in wind speed with subtle changes in blade pitch. For example, if the turbine detects a drop in wind speed, the blades may pitch back to generate more lift, but then if the wind speed increases quickly after, the blades will pitch forward again. If the blade pitch cannot immediately respond to increases in wind speed, then power losses occur. At these higher wind speeds, lower turbulence enables consistent blade pitch to match atmospheric conditions, and so the turbine can capture more power.

It is also important to mention the strong connection between turbulence and shear: high shear will eventually erode turbulence (Wharton and Lundquist 2012a). Periods of high shear generally coincide with periods of low turbulence and vice versa. With low shear, the mean wind speed is more consistent over the height of the rotor disk. However, since we did not see significant differences in power curves for different shear regimes here, we cannot speculate further on this in this analysis. Finally, if veer occurs in the wind profile (as in Vanderwende and Lundquist 2012 and Dörenkamper et al. 2015), which usually occurs only in stable or low turbulence atmospheric conditions, that veer will generally undermine power production as the turbine blades are not oriented perpendicular to the flow at all vertical levels."

Wind turbine power production and annual energy production depend on atmospheric stability and turbulence

Clara M. St. Martin,[1] Julie K. Lundquist,[1,2] Andrew Clifton,[2] Gregory S. Poulos,[3] and Scott J.

Schreck[2]

[1] Department of Atmospheric and Oceanic Sciences (ATOC), University of Colorado at Boulder, 311 UCB, Boulder, CO, 80309

[2] National Renewable Energy Laboratory, 15013 Denver West Parkway, Golden, CO, 80401

[3] V-Bar, LLC, 1301 Arapahoe Street, Suite 105, Golden, CO, 80401

Correspondence to: Clara M. St. Martin (clara.st.martin@colorado.edu)

Abstract. Using detailed upwind and nacelle-based measurements from a General Electric [GE] 1.5sle model with a 77-m rotor diameter, we calculated power curves and annual energy production (AEP) and explored their sensitivity to different atmospheric parameters to. This work provides guidelines for the use of stability and turbulence filters in segregating power curves. to gain a clearer picture of the power performance of a turbine. The wind measurements upwind of the turbine include anemometers mounted on a 135-m meteorological tower as well as profiles from a and lidar vertical profiles. We calculated power curves for different regimes based on turbulence parameters such as turbulence intensity (TI) and turbulence kinetic energy (TKE), as well as atmospheric stability parameters such as the Bulk Richardson number (R_B). We also calculate AEP was also calculated with and without these atmospheric filters and highlight differences between the results of these calculations. are highlighted in this article. The power curves for different TI and TKE regimes revealed that, at the U.S. Department of Energy (DOE) National Wind Technology Center (NWTC) at the National Renewable Energy Laboratory (NREL), increased TI and TKE underminesd power production at wind speeds near rated, but TI increasesd power production at lower wind speeds at this site, the U.S. Department of Energy (DOE) National Wind Technology Center (NWTC). Similarly, power curves for different R_B regimes revealed that periods of stable conditions produced more power at wind speeds near rated and periods of unstable conditions produced more power at lower wind speeds. AEP results suggest that calculations done without filtering for these atmospheric regimes may be overestimateing the AEP. Because of statistically-significant differences between power curves and AEP calculated with these turbulence and stability filters for this turbine at this site, we suggest implementing an additional step in analyzing power performance data to incorporate effects of take atmospheric stability and turbulence across the rotor disk. into account.

Keywords

wind energy, power curve, atmospheric stability, TI

1 Introduction

Calculating and understanding a wind turbine power curve is crucial for pPower performance testing and annual energy production (AEP) assessments rely on accurate calculations of wind turbine power curves. Previous work on power performance highlightsemphasizes the role of turbulence intensity (TI) and wind shear in influencing power production (Elliot and Cadogan, 1990; Hunter et al., 2001; Kaiser et al., 2003; Sumner and Masson, 2006; Gottschall

and Peinke, 2008; Antoniou et al., 2009; Rareshide et al., 2009; Wharton and Lundquist, 2012a, 2012b; Clifton et

al., 2013; Dörenkämper et al., 2014). Wharton and Lundquist (2012b) also found that vertical TI and turbulence

30   kinetic energy (TKE) affect power performance and Rareshide et al. (2009) found that veer affects power

performance. ~~Previous work also shows that a~~Atmospheric stability induces deviations of power from the

manufacturer power curve (MPC) (Motta et al., 2005; van den Berg, 2008; Vanderwende and Lundquist, 2012;

Wharton and Lundquist, 2012b). ~~. Some work has also focused on a~~ and atmospheric variations across the rotor disk

~~that~~can influence ~~the~~ power performance results (Sumner and Masson, 2009; Wagner et al., 2009; Choukulkar et al.,

35   2015).

        Because the power curve ~~is~~so closely impacts~~tied to~~ AEP, factors that influence ~~the~~ power performance

typically influence AEP calculations as well. As suggested by the works mentioned above, ~~T~~the two most closely

explored atmospheric factors with regard to AEP are TI and wind shear, but the existing studies do not agree on the

influence of TI and wind shear on AEP. The simulation-based study of Antoniou et al. (2009) found that low wind

40   shear supported high AEP. For low wind speeds, the highest AEP occurred during conditions of high TI, but at

higher wind speeds, the highest AEP occurred when TI was low. In contrast, based on~~their analysis of~~ data from a

number of wind farms in the continental United States, Rareshide et al. (2009) also compared AEP calculated with

different TI and shear combinations, and found that AEP typically decreased with increasing TI, but increased with

increasing shear.~~, in contrast to the findings of Antoniou et al. (2009)~~.

45   In this study, we also investigate~~d~~ the influence of different atmospheric stability and turbulence regimes

on wind turbine power curves and AEP calculations, incorporating a broad set of atmospheric parameters as well as

different approaches to measuring these parameters. In Sect. 2 we describe our data set, which includes an upwind

meteorological (met) tower with measurements spanning the rotor disk as well as a wind-profiling lidar. In Sect. 3

we present our data analysis methods, which include filtering the data by atmospheric parameters like shear, TI, and

50   atmospheric stability. The effects of atmospheric parameters on power curves and AEP are presented in Sect. 4, and

in Sect. 5 we summarize conclusions about the effects of atmospheric stability and inflow turbulence on power

curves and AEP calculations.

2 Data

2.1 Measurement site

55 The measurements used in this analysis were collected at the U.S. Department of Energy (DOE) National Wind Technology Center (NWTC, Fig. 1) at the National Renewable Energy Laboratory (NREL), located just south of Boulder, Colo., and about 5 km east of the Colorado Front Range (Clifton et al., 2013; Aitken et al., 2014). The prevailing wind direction at 80 m (hub height) at this site during this campaign (29 November 2012 – 14 February 2013) was west–northwesterly.

60 This wind direction also dominated a 14-year period from a neighboring met tower at the NWTC (Clifton and Lundquist, 2012). During the winter, the downslope flow from the nearby Rocky Mountains is frequently channeled through Eldorado Canyon, located just west–northwest of the NWTC (Banta et al., 1996; Poulos et al., 2000, 2007; Clifton et al. 2013; Aitken et al., 2014). The NWTC site slopes upward with about 20 m in elevation change toward the west for about 1.5 km before dropping off 20 m towards the highway on the western edge of the 65 site . The surface is mostly short grass.

2.2 Upwind measurements

Upwind measurements were taken using a Renewable NRG Systems (NRG)/LEOSPHERE WINDCUBE v1 vertically- profiling Doppler lidar (Courtney et al., 2008; Rhodes and Lundquist, 2013) and a 135-m met tower. The tower supportsincludes several levels of cup anemometers, vanes, sonic anemometers, and temperature sensors, 70 along with precipitation and air-pressure sensors (Fig. 2, Table 1), all on booms pointing in the dominant wind direction (west–northwest). Data were collected during the winter season, typically the season of theat times of strongest winds at the NWTC (from 29 November 2012 through 14 February 2013). The lidar is located about 215216 m (2.82.7D) west of the General Electric (GE) 1.5sle turbine on the NWTC site. The met tower is located about 170160 m (2.0.2D) west–northwest of the turbine (Fig. 1). Because different instruments employ different 75 averaging methods, Fig. 3 demonstratesshows that all wind speed data sets were synchronized and illustrates how the power output responds to changes in wind speed.

2.2.1 Lidar

The NRG/LEOSPHERE WINDCUBE v1 lidar measures volumetric-averaged wind speeds and directions every 20 m from 40 m to 220 m, thereby spanning the entire vertical extent of the turbine rotor disk. The wind speeds are

80 measured with an accuracy of 0.2 m s^{-1} and the wind directions are measured at an accuracy of 1.5° (Pauliac, 2009).

First, we filtered the nominally 1-Hz measurements of the horizontal wind speeds and directions for suitable carrier-to-noise ratio (CNR). Next, we averaged these 1-Hz data to 10-min averages for comparison with the tower and turbine data. The lidar takes a volumetric measurement, assuming homogeneity over the entire volume it is measuring. This process introduces an uncertainty in the lidar measurements in inhomogeneous flow (Bingöl et al.,

85 2009; Rhodes and Lundquist, 2013; Lundquist et al., 2015); this possible source of error is discussed in further detail in the supplement (Sect. S1).

2.2.2 Meteorological tower

The M5 met tower (NWTC, 2016, similar to the M4 tower at the site, which was studied by Rinker et al., 2016) is instrumented with cup anemometers at 3, 10, 30, 38, 55, 80, 87, 105, 122, and 130 m, and vanes at 3, 10, 38, 87, and

90 122 m (Fig. 2 and Table 1). Barometric pressure and precipitation sensors are located at 3 m and temperature sensors at 3, 38, and 87 m (Table 1). Sonic anemometers are mounted at 15, 41, 61, 74, 100, and 119 m (Fig. 2 and Table 1). The tower booms are directed at 278°, into the prevailing wind direction, slightly north of west. Measurements from the sonic anemometers at 15 ~~m~~ and 74 m are~~were~~ used to calculate turbulent fluxes of momentum and heat for assessment of atmospheric stability and turbulence as discussed in the following sections.

95 ### 2.3 Wind turbine data

A GE 1.5MW turbine (GE 1.5/77 sle) with an 80-m hub-height was chosen for this study. The GE 1.5MW is the most widely deployed utility-scale turbine in the world with more than 12,000 turbines deployed around the globe as of 2009 (GE Energy, 2009). The supervisory control and data acquisition (SCADA) system of the ~~DOE GE 1.5sle~~ turbine provides 10min averages of nacelle wind speed, nacelle orientation, turbine power, ~~and~~ blade pitch angles,

100 and generator set point values. These measurements can be compared with the upwind measurements to quantify power curves and AEP. The cup anemometer mounted on the nacelle of the turbine is a NRG IceFree Hybrid XT Turbine Control Anemometer. The GE 1.5sle reaches its nameplate capacity, 1.5 MW, at a wind speed of 14 m s^{-1} (GE Energy, 2009). We refer to this wind speed as the rated wind speed for the rest of this article. The lower and upper extremes of the swept area of the GE 1.5sle in this study are approximately ~~were~~ 41.5 m and 118.5 m above

105   ground. More details on this turbine and power performance testing results as well as instrument and site calibration

information can be found in Mendoza et al. (2015).

3 Analysis methods

Before calculating atmospheric parameters, all meteorological and turbine data ~~are~~were checked for data quality as

described in Sect. 3.1.

110   **3.1 Data quality control**

3.1.1 Lidar

All lidar-measured wind-speed measurements ~~are~~were filtered by CNR: only measurements with a CNR greater than

−18 dB ~~are~~were retained. Lower CNR results from clean-air conditions (Aitken et al., 2012), which occur frequently

on Colorado's Front Range in the winter. After additional filtering for quality control purposes (such as removing

115   bad data as defined by the manufacturer's wind speed and temperature limits), the data recovery rate ~~is~~was

approximately 33.5 % for horizontal wind speeds and directions at 40 m, 40 % for horizontal wind speeds and

directions at 60 and 120 m, and 45 % for horizontal wind speeds and directions at 80 and 100 m.

3.1.2 Meteorological tower

Quality control filtering methods performed on the met tower data ~~followed procedures including~~ discard~~ing~~ data

120   that ~~are~~were flagged for a number of reasons, including~~because of~~ irregular timing (~~when~~ the time between

measurements ~~is~~was inconsistent), insufficient percentage~~number~~ of data points within a~~n~~ ~~10min~~ averaging period

(less than 95 %)~~according to the manufacturer~~, low standard deviation (less than 0.01 % of the mean) or constant

values during the measurement interval (which indicate icing events), empty data channels, bad values as defined by

manufacturer limits, or when an instrument record~~s~~ed a "NaN" in place of a real measurement. After filtering for

125   quality control purposes, the met tower provides~~measured~~ horizontal wind speeds and directions and temperatures

about 90 % of the time at all levels during this study.

       Several spikes in wind speed occur in the raw sonic anemometer data. Therefore, a de-spiking filter is

applied based on the change in wind speed from each data point to the next. Data points are removed if they are

preceded and followed by changes exceeding the lowest 99 % of all changes. After filtering the spikes in the sonic

130   anemometers as well as the previously discussed quality control procedure, the sonic anemometers provide wind speed and temperature about 90 % of the time at 15 m and about 60 % at 74 m during this study.

3.2 Wind speed and direction subselection

Although the dominant wind direction at the site is west-—northwesterly, other wind directions do occur. To ensure the lidar and met tower measurements are were wake-free (upwind of the turbine), we considered only data from

135   time periods of hub-—height wind from the 235°–315° wind direction sector. This sector includes the most frequent and highest wind speeds as measured by both upwind instruments (Fig. 4). Only wind speeds between cut-in (3.5 m s^{-1}) and cut-out (25 m s^{-1}) are were considered to ensure that the turbine is was operating.

3.3 Filtering turbine underperformance

After filtering for quality control as well as wind speed and direction, we still saw a large number of times occur

140   when the turbine was is producing significantly less power than expected—underperforming— relative to most of the points, as seen in Fig. 5a. However, blade pitch angles can be used to segregate data and flag most of these underperforming periods, as follows. We test two methods to isolate and discard the cases where the turbine is producing significantly lower power, inconsistent with "normal operation." The first approach relies on blade pitch angle to segregate data and flag most of these underperforming periods; this approach could be used by wind plant

145   owner-operators with access to limited SCADA parameters. When more SCADA parameters are available, such as generator set point values, these values may be used in a more rigorous way to filter on curtailment and to define normal turbine operation.

3.3.1 Filtering based on blade pitch angle

Without access to the turbine control system or data more refined than 10-min averages, typical blade pitch angles

150   can be quantified as a function of wind speed (Fig. 5b). The median value for blade pitch angle for each wind speed bin as well as $\pm$ 4.5 3 median absolute deviation (MAD), equivalent to 3 σ, are shown by the red envelope in Fig. 5b. (We used MAD here instead of mean absolute deviation so that the calculation is not biased by a few outliers would not bias the calculation.) When plotted on a power curve using the tower 80-m cup anemometer for wind speed, Fig. 5a, the majority of the points outside of the $\pm$ 4.5 3 MAD envelope and between 5 and 17 m s^{-1} showed

155   underperformance. To identify filter for underperformance, then, we calculated MAD blade pitch angles from each

blade for each wind speed bin between 5 and 17 m s^{-1}. Time periods with blade pitch angle~~s~~s outside of $\pm$ 4.5~~3~~ MAD ~~are~~were discarded. ~~Although it is possible that~~While variability on timescales shorter than 10 min may affect turbine operation, the effective filtering seen in the red~~magenta~~ scatter in Fig. 5a suggests that this approach is sufficient. This filtering by blade pitch angle also has the advantage of using only data to which a typical wind plant operator would have access.

After filtering for hub–height wind speed and direction, positive power production, and blade pitch angle, ~~1,214~~1,240 out of 7,949 lidar 80-m wind speed data points remain~~ed~~ (~~15~~16 %), and ~~2,196~~2,235 out of 9,918 met tower 80-m wind speed data points remain~~ed~~ (~~20~~23 %). Concurrent lidar, met tower, and turbine data that fulfill~~ed~~ the various screening criteria occur~~red~~ during ~~1,083~~1,107 10-min periods.

3.3.2 Filtering based on extensive SCADA turbine operational parameters

Access to a number of turbine control parameters from the SCADA on the DOE GE 1.5 allows for a more accurate definition of normal turbine operation, mostly based on generator set point values and filtered on curtailment. However, from cut-in wind speed until around 5.5 m s^{-1}, using generator set point to filter the data results in discarding too many data points. Therefore, between cut-in wind speed and about 5.5 m s^{-1}, the generator set point is not used; rather data points are discarded only when the turbine is not grid connected and is faulted. Above 5.5 m s^{-1}, only generator set point is used to filter on curtailment and for normal operation. The data points filtered using this method are represented in Figure *6* in blue, while the red points in Figure *6* represent the data points that pass this filtering method.

After filtering for hub-height wind speed and direction, positive power production, and normal turbine operation, 1,227 out of 7,949 lidar 80-m wind speed data points remain (15 %), and 2,249 out of 9,918 met tower 80-m wind speed data points remain (23 %). Concurrent lidar, met tower, and turbine data that fulfill the various screening criteria occur during 1,127 10-min periods.

3.3.3 Comparison of different turbine operation filters

The normal turbine operation filters described in Sect. 3.3.2 not only filter out all of the times when the turbine is producing significantly less power than expected, but allows the use of about 2 % more data points deemed "bad" by the blade pitch angle filtering method described in Sect. 3.3.1. Many of the data points that would be discarded using

the blade pitch angle filtering method are between cut-in wind speed and 10 m s^{-1}, and lie reasonably within the expected power curve, on top of data points that passed through the filter. Therefore, the remaining analysis is based on data filtered using the methodology described in Sect. 3.3.2.

3.4 Power curves

Power curves based on wind speeds normalized by air density following International Electrotechnical Commission (IEC) 61400-12-1 (2015) can be used to evaluate turbine performance. The observed power curves, comparing power production to 80-m tower anemometer wind speeds (Fig. 6a7a), 80-m lidar wind speeds (Fig. 6b7b), and nacelle anemometer wind speeds (Fig. 6c7c), generally showed good agreement with an approximation of the MPC (GE Energy 2009). This approximated MPC iswas determined by placing the publically available MPC for the GE 1.5sle on a grid (with dimensions of 0.5 m s^{-1} by 50 kW) and estimating expected power produced at each wind bin.

The nacelle-mounted anemometer does not observe the ambient wind speed that the rotor disk experiences because the wind that flows through the rotor disk and along the nacelle during operation is modified by the blades and nacelle (Antoniou and Pedersen 1997; Smith et al. 2002; Frandsen et al. 2009; Zahle and Sørensen 2011). However, power curves calculated using nacelle wind speeds are shown here along with power curves calculated using upwind measurements in order to compare the different methods. In many cases, operators calculate these nacelle-based power curves due to lack of other data.

The power curves created from 10-min tower and nacelle-mounted anemometers (Fig. 6a7a, Fig. 6c7c, respectively) showed less variability than the lidar power curve (Fig. 6b7b). It is especially apparent from the power curve created from 10-min lidar measurements (Fig. 6b7b) that the lidar variability at this particular site is vulnerable to inhomogeneity in the flow. Although lidars are widely available and used in the field (Clifton 2015), the variability between the lidar and tower measurements (Fig. 78) indicatesd sufficient inhomogeneity in the flow at this particular site (as observed by Aitken et al., 2014) to cause us to discuss and show only the upwind data from the tower from this point forward. Note, however, that not all sites are subject to the inhomogeneity seen at the NWTC, and all instruments available for wind measurement should be considered. Concurrent met tower and turbine data that fulfilled the screening criteria occurred during 2,1862,240 10-min periods, equivalent to about 364373 h of data, which is more than twice the 180 h of data that the IEC 61400-12-1 standard (2015) recommends for power performance testing.

3.5 Atmospheric stability regimes

210   Numerous approaches are available for classifying the atmospheric stability of a given 10-min or 30-min time period. Bulk Richardson number (R_B) calculations use temperature and wind speed differences from the lowest met tower measurement to the height of the top of the rotor disk to compare the buoyant production of turbulence to the wind-shear-generated mechanical production of turbulence (Stull, 1988) as

$$R_B = \frac{g\,\Delta T\,\Delta z}{\bar{T}\,\Delta U^2} \; , \tag{1}$$

215   where g is the gravitational constant 9.81 m s^{-2}, Δz is the change in height, ΔT is the change in 10-min averages of temperature across Δz, $\bar{T}$ is the mean temperature across Δz, and ΔU is the change in the 10-min averages of horizontal wind speed across Δz. Note that Eq. (1) does not consider wind direction variability because cup anemometer measurements provide only information about horizontal wind speed. Typical stability classifications based on R_B calculations are as follows: turbulent flow in unstable conditions when R_B is less than 0, laminar flow

220   in stable conditions when R_B is greater than 0.25, and neutral conditions when R_B is between 0 and 0.25 (Stull, 1988). These stability classifications are similar to those used in previous work on stability effects on wind turbine fatigue and loading in Kelley (2011), and slightly different from the stability classifications used in Vanderwende and Lundquist (2012). The distribution of R_B calculated from the tower measurements for this campaign (Fig. 8̶9), however, suggested that slightly different regimes, shown in Table 2, could be used to better represent the data at

225   this site. R̶_B̶ ̶r̶e̶g̶i̶m̶e̶s̶ ̶a̶r̶e̶ ̶s̶i̶m̶i̶l̶a̶r̶l̶y̶ ̶d̶e̶f̶i̶n̶e̶d̶ ̶f̶o̶r̶ ̶t̶h̶e̶ ̶N̶W̶T̶C̶ ̶i̶n̶ ̶A̶i̶t̶k̶e̶n̶ ̶e̶t̶ ̶a̶l̶.̶ ̶(̶2̶0̶1̶4̶)̶.̶ Similar to the approach used in Aitken et al. (2014), the R_B distribution id split roughly into thirds to allow for less overlap between stable and unstable regimes. The uncertainty in R_B for these instruments over the measurement period is about 0.01, therefore the R_B classifications used are larger than the uncertainty.

      Obukhov length *(L)* is also a useful measure of atmospheric stability, relying on surface stresses as well as

230   heat fluxes to estimate the height in the surface layer at which the buoyant production of turbulence dominates wind-shear-generated mechanical production of turbulence (Stull, 1988) as

$$L = -\frac{u_*^3}{k\,g}\,\frac{T_v}{\overline{w'T_s'}} \; , \tag{2}$$

where u_* is the friction velocity, k is the von Karman constant 0.4~~1~~, T_v is the virtual temperature, w' is the vertical wind speed fluctuation in the ~~10~~30-min averaging period, and T_s' is the sonic temperature fluctuation in the ~~10~~30-min averaging period. *L calculations are based on sonic anemometer measurements at 15 m and temperature measurements interpolated to 15 m to ensure L is calculated using measurements within the surface layer.* Typical stability classifications are used in this work and are based on L calculations as defined by Muñoz-Esparza et al. (2012); shown in Table 2. These classifications are slightly different from those used in Wharton and Lundquist (2012b). The distributions of L are shown in Fig. ~~9~~10.

When the R_B and L stability approaches are compared against one another and against time-of-day, as in Fig. ~~10~~11, the ~~different~~ stability parameters differ slightly in their definitions of unstable and stable. Because of differences in stability classes ~~using these different stability parameters, along with their~~ due to varying~~different~~ approaches to defining atmospheric stability, we treat~~ed~~ R_B-defined stability classes separately from L-defined stability classes in the power curves.

3.6 Turbulence regimes

TI can also be used to describe atmospheric conditions, as demonstrated by Rareshide et al. (2009), Wagenaar and Eecen (2011), and Wharton and Lundquist (2012a). TI is typically defined as

$$TI = \frac{\sigma_{80m}}{U_{80m}} * 100 ~~-~~,$$ (3)

where σ_{80m} is the 10-min standard deviation of the horizontal wind speed at 80 m and U_{80m} is the 10-min mean horizontal wind speed at 80 m. Although the TI approach has been used successfully at other locations, the NWTC consistently features strong turbulence likely resulting from the terrain characteristics of the site (Fig. ~~11~~12, Fig. ~~Figure~~ 13), making it difficult to distinguish typical stability classes from TI calculations. This strong ambient turbulence has led to the choice of site-specific turbulence classification defined in Table 3.

When the atmospheric stability regimes are compared to the TI regimes defined here (Fig. ~~13~~14), the R_B and TI regime percentages also differ slightly in their definitions of unstable atmospheric conditions and highly turbulent conditions. Most of the daytime points are within the unstable regime as defined by R_B; however, only

about ~~16~~17 % of the data fall within unstable conditions with higher TI. This comparison, again, emphasizes the highly turbulent characteristics of the NWTC.

To further understand the turbulence characteristics demonstrated during this campaign, we also calculate~~d~~ TKE using the 74-m 3D sonic anemometer mounted on the M5 met tower. Although TI is a parameter typically calculated and analyzed in the wind industry, TKE has the advantage of including the vertical component of the wind:

$$TKE = \frac{1}{2}\left(\overline{u'^2} + \overline{v'^2} + \overline{w'^2}\right) \ , \tag{4}$$

where we calculate TKE per unit mass, u' is the perturbation from a ~~10~~30-min average of the ~~u~~zonal -component of the wind, v' is the perturbation from a 30~~10~~-min average of the ~~v~~meridional -component of the wind, and w' is the perturbation from a ~~10~~30-min average of the ~~w~~vertical -component of the wind. Using this TKE approach also revealed the strong turbulence at the NWTC. only slightly affected by the ~~with little or no~~ diurnal cycle during this wintertime campaign (Fig. ~~11~~12, Fig. ~~14~~15). Turbulence classifications based on TKE are~~were~~ determined by the distribution in Fig. ~~14~~15 and are listed in Table 3.

Many cases with relatively high TI or TKE are considered neutral and stable according to our stability definitions in Table 3. Depending on whether TI, TKE, R_B, or L is considered a measure of atmospheric stability, a particular time period may be classified differently. In other words, different results are found depending on the metric selected.

3.7 Wind shear regimes

To estimate the effect of the wind speed vertical profile across the rotor disk, the wind shear exponent or power law exponent parameter, α, is typically used in the wind energy industry:

$$\alpha = \frac{\log\left(\frac{U_2}{U_1}\right)}{\log\left(\frac{z_2}{z_1}\right)}, \tag{5}$$

where z_1 is the reference height, z_2 is the height above ground level, U_2 is the wind speed at height z_2, and U_1 is the wind speed at height z_1. At the NWTC during this study, the average wind shear exponent using the 122 m and 38 m

280   tower wind speeds as z_2 and z_1-, respectively, is 0.15. The standard deviation is 0.14 and the maximum wind shear

exponent is 1.10, however.

For this period of time at this site, however, it was rare for the rotor equivalent wind speed (REWS) to
deviate significantly from the hub-height wind speed (Sect. S2). Therefore, shear exponents are separated into
regimes simply by splitting the shear exponent distribution into thirds (Table 2, Fig. 16). Other approaches to

285   classify stability regimes using shear exponents such as combining with other stability measures such as L and R_B
(Vanderwende and Lundquist, 2012) or using a REWS in the power curves (Elliott and Cadogan, 1990), may work
at other sites.

Although we found no statistically significant impact of wind shear on the power curves at this site, we did
include shear exponent in the subsequent analysis, separating regimes of shear exponent as defined in Table 2 and

290   based on the distribution in Fig. 15.

4 Results

To explore the variability in the power curves, we applyied filters to the power curves based on factors such as
atmospheric stability and, TI, and TKE. We applyied a new method to calculate AEP using these classifications. We
can consider periods with low TI or TKE to be approximately "stable" by R_B and L; "unstable" conditions would

295   generally have high TI and TKE. Our results showed that, generally, at this site with little veer, stable conditions
(with varying degrees of significance) lead to over-performance at wind speeds just below rated power. At lower
wind speeds, however, Uunstable conditions lead to over-performance, at lower wind speeds with a few exceptions.

4.1 Power curves

The NWTC site generally exhibitsed high TI throughout this data collection period. Even so, some differences in

300   power produced emerged at wind speeds between 5 and 7 m s^{-1} and at wind speeds between 10 and 14 m s^{-1} after
separating the TI into relative classes of low, medium, and high TI (Fig. 16a17a, Fig. 16d17c, Fig. 17a18a, Fig.
17d18c, Table 3). Statistically-distinct differences within each wind speed bin between the TI classes defined in
Table 3 arewere determined by the Wilcoxon rank sum test with a 1 % significance level. These statistically–distinct
bins are denoted by closed circles in Fig. 16a17a, Fig. 16d17c, Fig. 17a18a, and Fig. 17d18c. This statistical test

305   shows that for the power curves using nacelle winds, periods of relatively high TI produce significantly more power

than periods of relatively low TI at wind speeds between 5 and 9 m s^{-1} (Fig. ~~16a~~17a, Fig. ~~17a~~18a). For the power

curves using upwind tower winds, periods of relatively high TI produce significantly more power than periods of

relatively low TI at wind speeds between 6.0~~5~~ and 6.5 m s^{-1} (Fig. ~~16d~~17c, Fig. ~~17d~~18c). Conversely, power curves

using nacelle winds show that at wind speeds between 10.5 and 13.5 m s^{-1}, periods of relatively low TI produce

310   significantly more power than periods of relatively high TI. Power curves using upwind tower winds show that at

wind speeds between 9.5 and 15.5 m s^{-1}, periods of relatively low TI produce significantly more power than periods

of relatively high TI. Rareshide et al. (2009) found similar behavior.

On the other hand, power curves separated by R_B-defined stability class show only a few bins that are

statistically distinct in power produced (Fig. ~~16b~~17b, Fig. ~~16e~~17d, Fig. ~~17b~~18b, Fig. ~~17e~~18d). Power curves using

315   nacelle winds show that at some wind speeds between 6.5~~5.5~~ and 9.0 m s^{-1}, periods of unstable conditions produce

significantly more power than periods of stable conditions. Power curves using upwind tower winds show that at

wind speeds around 7 m s^{-1}, periods of unstable conditions produce significantly more power than periods of stable

conditions. Power curves using both nacelle winds and tower winds show that at wind speeds around 12 m s^{-1},

periods of stable conditions produce significantly more power than periods of unstable conditions.

320   ~~Similarly, Fig. 16c, Fig. 16f, Fig. 17c, and Fig. 17f show periods of low TKE producing significantly more~~

~~power at wind speeds just before rated than periods of high TKE, similar to the TI and R_B methods. Between 7.5 and~~

~~9.5 m s^{-1}, power curves using nacelle winds show that periods of high TKE produce significantly more power than~~

~~periods of low TKE. Interestingly, however, power curves using upwind tower winds show that at 4 m s^{-1}, just after~~

~~cut-in, periods of low TKE produce more power than periods of high TKE.~~

325   Distinct differences between power curves calculated from nacelle winds and power curves calculated from

upwind tower winds occurred in the power curves of both~~all three~~ of these atmospheric parameters. Statistically

distinct wind speed bins in power curves calculated from nacelle winds tend~~ed~~ to be similar to those in power curves

calculated from tower winds near rated speed. At lower wind speeds, however, between about 5 and 9 m s^{-1}, many

more statistically distinct differences emerge~~d~~ between nacelle power curves than between tower power curves,

330   most notably in the power curves segregated by TI regimes. Turbine operations are~~were~~ especially variable in this

region of rapid increase in power with wind speed. The turbine reacts~~ed~~ directly to the conditions as measured by

instruments on the turbine. The nacelle-mounted anemometer observes winds that flow through the rotor disk and

along the nacelle during turbine operation, and therefore likely measures different wind speeds than the upwind met tower. The nacelle anemometer observes complex flows behind the rotor disk that are strongly influenced by ambient turbulence, leading to more statistically significant differences in the nacelle power curves for TI regimes.

Agreement between the TI and, R_B, and TKE methods means that at wind speeds around rated, low TI, high stability, and low TKE result in over-performance relative to high TI and, low stability, and high TKE. BothAll three methods also agree that somewhere in between cut-in and rated, sometimes called "region 2," high TI and, low stability, and high TKE result in over-performance relative to low TI, and high stability, and low TKE. Power curves separated by L-defined stability class as well as power curves separated by shear class do not show any statistically-significant differences in power produced between unstable and stable periods (not shown). Power curves separated by TKE class show few statistically-significant differences in power produced between high and low TKE periods, likely because of the few data points available for the 30-min averaging period, therefore these results are shown in the supplement (Sect. S4).

4.1.1 Underlying physics

The large variability reported in the literature (and herein) regarding power production can be understood by recognizing the interactions between a pitch-controlled turbine and the atmosphere: the operation of control algorithms changes with wind speed, with varying effects depending on the ambient turbulence.

Sensitivity to atmospheric turbulence occurs at low wind speeds, near cut-in wind speed. In these conditions, the turbine generator speed (revolutions per minute, RPM) increases, as does the generator torque. As a result, the blades will often pitch backward, changing the angle of attack to generate more lift, and the power production ramps up. At low wind speeds and higher turbulence, the turbine can react to the higher variation in wind speed and can capitalize on the variation seen in the wind flow because of the additional lift resulting from the blade pitch, and the turbine produces more power. Conversely, at low wind speeds with lower turbulence, the variation in wind speed is lower, and so the turbine experiences more consistent wind than in highly turbulent conditions and therefore produces less power.

At higher wind speeds, closer to or just below rated speed, control mechanisms seek to maintain rated generator speed, rather than continuing to increase generator speed. The blades will pitch forward (or "feather"),

allowing the power production to maintain rated power. This process effectively decreases the amount of lift when
compared to lift generated by a non-feathered blade. At these wind speeds during periods of high TI, a turbine
reacts to the high variation in wind speed with subtle changes in blade pitch. For example, if the turbine detects a
drop in wind speed, the blades may pitch back to generate more lift, but then if the wind speed increases quickly
after, the blades will pitch forward again. If the blade pitch cannot immediately respond to increases in wind speed,
then power losses occur. At these higher wind speeds, lower turbulence enables consistent blade pitch to match
atmospheric conditions, and so the turbine can capture more power.

It is also important to mention the strong connection between turbulence and shear: high shear will
eventually erode turbulence (Wharton and Lundquist, 2012a). Periods of high shear generally coincide with periods
of low turbulence and vice versa. With low shear, the mean wind speed is more consistent over the height of the
rotor disk. However, since we did not see significant differences in power curves for different shear regimes here,
we cannot speculate further on this in this analysis. Finally, if veer occurs in the wind profile (as in Vanderwende
and Lundquist, 2012 and Dörenkamper et al., 2015), which usually occurs only in stable or low turbulence
atmospheric conditions, that veer will generally undermine power production as the turbine blades are not oriented
perpendicular to the flow at all vertical levels.

4.2 Annual energy production

AEP allows developers and operators to quantify the projected energy production of a turbine. To quantify the
impact on AEP of these stability- and turbulence-driven differences in power curves, we used a Weibull distribution
for wind speed and calculated AEP with no filter, as well as with TI, shear, and stability filters. These turbulence
and stability filters for the AEP calculations can be further explained as AEP calculated using the power curves
calculated from nacelle winds (Fig. Figure a,b) as well as the power curves calculated from upwind tower winds
shown in (Fig. 1617c,d). These power curves are used together with a sample wind distribution using Weibull
distribution parameters based onrepresentative of wind speed data separated into each stability class (Table 4) the
data set ($\lambda = 10.13$ m s^{-1}, $k = 2.62$) as suggested by IEC 61400 12-1 (2015) for a site-specific AEP. For each of these
filters, separate AEP calculations arewere made for each regime, weighted by the number of data points in that
regime, and then added together to compare with the AEP calculated with no atmospheric filter. Note that although

385 data ~~were~~ are collected only during 2.5 months in the winter of 2012, AEP ~~was~~ is calculated for an entire year to show values closer to a representative AEP value.

Results in Table ~~4~~ 5 show a higher AEP when using no filter, followed by an AEP calculated with a TI filter and then a ~~shear~~ stability filter. ~~Although it is shown in the power curves in Fig. 16 and Fig. 17, a TKE filter to calculate AEP is not presented here because the result was a significantly smaller AEP, most likely resulting from the lack of data points in comparison to the other filters.~~ The lower AEP calculated when separating by stability and

390 turbulence regimes suggests that the AEP calculated using no filters may be overestimating the production, perhaps because the higher and lower extremes of the parameter ranges bias the averages in each bin.

AEP results in Table 5 also show that the AEP calculated using nacelle winds underestimates the AEP when compared with an AEP calculated using upwind tower measurements. This underestimation of the nacelle

395 anemometer-calculated AEP is true for both the AEP calculated for the entire dataset as well as with each stability or turbulence filter and is likely because the nacelle anemometer underestimates the ambient wind speed due to flow interference of the rotor disk and nacelle.

When the AEP's low and high regimes are compared to the medium regimes of their respective atmospheric parameters, the AEP for medium-TI periods is higher than that for low-TI periods and for high-TI

400 periods for both the nacelle anemometer-calculated AEP and the tower-calculated AEP (Table ~~5~~ 6). Using low- and high-TI power curves results in an AEP smaller than that calculated using the medium-TI power curve. These results are likely obtained because the low-TI power curve loses production at lower wind speeds and the high-TI power curve loses production around rated speed. ~~When using a shear filter, the AEP calculated with the high-shear power curve is higher than that with the low-shear power curve (Table 5). Conversely,~~ ~~W~~when using a stability filter, the

405 AEP calculated with the low-R_B power curve is higher than that with the high-R_B power curve (Table ~~5~~ 6). This contrast between AEP calculated for the low stability regime and AEP calculated for the high stability regimes suggests that the unstable power curve (Fig. ~~16b~~ 17b,d) gains enough production near rated wind speed to surpass the production gain by the stable power curve (Fig. ~~16b~~ 17b,d) at lower wind speeds.

5 Conclusions

Using 2.5 months of data from upwind and nacelle-based instruments, we calculate~~d~~ power curves for different regimes of atmospheric stability and turbulence as well as AEP with and without these atmospheric filters. This work focuses not only on the idea of calculating different power curves for different atmospheric conditions for power performance testing, but also highlights the differences in AEP that can emerge from the application for stability- or turbulence-dependent power curves. We summarize extensive data quality–control methods, including two approaches for filtering out turbine underperformance or curtailments.

Statistically-~~-~~significant differences emerge among power curves segregated by TI~~, TKE,~~ and R_B. At wind speeds between 5 and 7 m s^{-1}, during periods of high TI, significantly more power is produced than during periods of low TI. From about 10 to 14 m s^{-1} (near rated wind speed), during periods of low TI, significantly more power is produced than during periods of high TI. ~~Similarly, periods of high TKE produce significantly more power between 7.5 and 9.5 m s^{-1} than during periods of low TKE, and periods of low TKE produce significantly more power around 12 m s^{-1} than during periods of high TKE.~~ During periods of stable conditions, significantly more power is produced than during periods of unstable conditions around 12 m s^{-1}; significantly less power is produced than during periods of unstable conditions at some wind speeds between ~~5.5~~6.5 and 9.0~~8.5~~ m s^{-1}. Statistically significant distinctions in power curves did not occur when filtering for TKE, L, yaw error, wind shear, or wind veer for this data set at this site, perhaps explaining why stable conditions promote overperformance here, as in Wharton and Lundquist (2012b). A site with veer, however, exhibits underperformance in stable conditions (Vanderwende and Lundquist 2012).

After calculating an AEP for each regime and comparing the high and low regimes with the medium regime, differences between AEP calculated using different atmospheric filters are revealed. An AEP calculated with no atmospheric or turbulence filter is higher than any AEP calculated with these filters. In addition, the AEP calculated using a TI filter shows that the AEP calculated with the medium TI regime is greater than the AEP calculated with the low or high TI regimes. The AEP calculated with the ~~shear filter shows that the high regime AEP is higher than the AEP in the low and medium regimes; the AEP calculated with the~~ R_B filter shows that the low regime AEP is much larger than the AEP in the high and medium regimes.

435   As a small percent difference in AEP leads to a large deviation in cost for both operators and manufacturers, calculating different power curves for different atmospheric conditions may not only be a practical approach, but may lower the financial risks for both operators and manufacturers.

As discussed by Rareshide et al. (2009), manufacturers are increasingly filtering out data that represent what they consider anomalous or extreme atmospheric conditions for power performance testing. The IEC-61400-
440   12-1 standard (2015) calls for at least 180 h of data to be used in a power performance test. Consequently, if manufacturers filter out data based on higher TI values, for instance, this means that more data must be gathered to make up for the discarded data. We see this discarding of data as unnecessary and potentially more costly. We suggest that instead of discarding these data, different power curves be calculated for different conditions. This approach canwill allow for a more nuancedrefined understanding of how athe turbine is operatesing in different
445   atmospheric conditions, and may lead to a more accurate and reliable performance result and AEP calculation.

Acknowledgements

The authors express appreciation to the Center for Research and Education in Wind for supporting this work, to Thomas Fischetti and Peter Gregg at GE Power & Water Renewable Energy for histheir assistance in turbine data collection and interpretation, and to the reviewers of a previous version of this work. This work was supported by
450   the U.S. Department of Energy under Contract No. DE-AC36-08GO28308 with the National Renewable Energy Laboratory. Funding for the work was provided by the DOE Office of Energy Efficiency and Renewable Energy, Wind and Water Power Technologies Office.

The U.S. Government retains and the publisher, by accepting the article for publication, acknowledges that the U.S. Government retains a nonexclusive, paid-up, irrevocable, worldwide license to publish or reproduce the published
455   form of this work, or allow others to do so, for U.S. Government purposes.

References

Aitken, M.L., Lundquist, J.K., Pichugina, Y.L., and Banta, R.M.: Quantifying wind turbine wake characteristics from scanning remote sensor data, J. Atmos. Ocean. Tech., 31, 765–787, doi:10.1175/JTECH-D-13-00104.1, 2014.

460   Aitken, M.L., Rhodes, M.E., and Lundquist, J.K.: Performance of a wind-profiling lidar in the region of wind turbine rotor disks, J. Atmos. Ocean. Tech., 29, 347–355, doi:10.1175/JTECH-D-11-00033.1, 2012.

Antoniou, I., and Pedersen, T.F.: Nacelle Anemometry on a 1MW Wind Turbine, Risø National Laboratory, Roskilde, Denmark, 37 pp., 1997.

465   Antoniou, I., Pedersen, S.M., and Enevoldsen, P.B.: Wind shear and uncertainties in power curve measurement and wind resources, Wind Engineering, 33, 449–468, doi:10.1260/030952409790291208, 2009.

Banta, R.M., Oliver, L.D., Gudiksen, P.H., and Lange, R.: Implications of small-scale flow features to modeling dispersion over complex terrain, J. Appl. Meteorol. , 35, 330–342, 1996.

Bingöl, F., Mann, J., and Foussekis, D.: Conically scanning LIDAR error in complex terrain, Meteorologische Zeitschrift, 18, 189–195, doi:10.1127/0941-2948/2009/0368, 2009.

470   Choukulkar, A., Pichugina, Y., Clack, C.T.M., Calhoun, R., Banta, R., Brewer, A. and Hardesty, M.: A new formulation for rotor equivalent wind speed for wind resource assessment and wind power forecasting, Wind Energy, 19, 1439-1452, doi: 10.1002/we.1929, 2016~~5~~.

Clifton, A. Remote sensing of complex flows by Doppler wind lidar: issues and preliminary recommendations, NREL, Golden, Colo., 1–42, 2015.

475   Clifton, A., Kilcher, L., Lundquist, J. K., Fleming, P.: Using machine learning to predict wind turbine power output, Environ. Res. Lett., 8, 8 pp., doi: 10.1088/1748-9326/8/2/024009, 2013.

Clifton, A., and Lundquist, J.K.: Data clustering reveals climate impacts on local phenomena, J. Appl. Meteorol. Clim., 51, 1547–1557, doi:10.1175/JAMC-D-11-0227.1, 2012.

Clifton, A., Schreck, S., Scott, G., and Lundquist, J.K.,: Turbine inflow characterization at the National Wind
480   Technology Center, J. Sol. Energ.-T ASME, 135, doi:10.1115/1.4024068, 2013.

Courtney, M., Wagner, R., and Lindelöw, P.: Testing and comparison of LIDARs for profile and turbulence measurements in wind energy, IOP Conference Series Earth and Environmental Science, 1, 1–14, doi:10.1088/1755-1307/1/1/012021, 2008.

Dörenkämper, M., Tambke, J., Steinfield, G., Heinemann, D., and Kühn, M.: Atmospheric impacts on power curves
485   of multi-megawatt offshore wind turbines, Journal of Physics: Conference Series, 555, 1–11, doi: 10.1088/1742-6596/555/1/012029, 2014.

Elliott, D.L., and Cadogan, J.B.: Effects of wind shear and turbulence on wind turbine power curves, Proc. European Community Wind Energy Conference and Exhibition, Madrid, Spain, 1990.

Frandsen, S., Sørensen, J.N., Mikkelsen, R., Pederesen, T.F., Antoniou, I., and Hansen, K.: The generics of wind
490   turbine nacelle anemometry, Proceedings of European Wind Energy Conference, Marseille, France, 2009.

GE Energy: 1.5 MW wind turbine, 2009, http://geosci.uchicago.edu/~moyer/GEOS24705/Readings/GEA14954C15-MW-Broch.pdf, last access: 21 January 2013.

Gottschall, J., and Peinke, J.: How to improve the estimation of power curves for wind turbines, Environ. Res. Lett., 3, 1–7, doi: 10.1088/1748-9326/3/1/015005, 2008.

495   Hunter, R., Pedersen, T.F., Dunbabin, P., Antoniou, I., Frandsen, S., Klug, H., Albers, A., and Lee, W.K.: European wind turbine testing procedure developments: Task 1: measurement method to verify wind turbine performance characteristics, Risø National Laboratory, Roskilde, Denmark,1–120, 2001.

IEC 61400-12-1 Ed 2.0: Wind turbines – Part 12-1: power performance measurements of electricity producing wind turbines, IEC, Geneva, Switzerland, 2015.

500   Kaiser, K., Hohlen, H., and Langreder, W.: Turbulence correction for power curves, Wind Energy Proc. European Wind Energy Conference and Exhibition, Madrid, 159–162, 2003.

Kelley, N.D.: Turbulence-turbine interaction: the basis for the development of the TurbSim Stochastic Simulator, NREL, Golden, Colo., 2011. http://www.nrel.gov/docs/fy12osti/52353.pdf, last access: 8 May 2016.

Lundquist, J.K., Churchfield, M.J., Lee, S., and Clifton, A.: Quantifying error of lidar and sodar Doppler beam
505   swinging measurements of wind turbine wakes using computational fluid dynamics, Atmospheric Measurement Techniques, 8, 907–920, doi: 10.5194/amt-8-907-2015, 2015.

Mendoza, I., Hur, J., Thao, S., Curtis, A.: Power performance test report for the U.S. Department of Energy 1.5-megawatt wind turbine, NREL, Golden, Colo., 1–55, 2015, last access: 8 May 2016, http://www.nrel.gov/docs/fy15osti/63684.pdf.

510   Motta, M., Barthelmie, R.J., and Vølund, P.: The influence of non-logarithmic wind speed profiles on potential power output at Danish offshore sites, Wind Energy, 8, 219–236, 2005.

Muñoz-Esparza, D., Cañadillas, B., Neumann, T., and vanBeech, J.: Turbulent fluxes, stability and shear in the offshore environment: mesoscale modelling and field observations at FINO1, Journal of Renewable and Sustainable Energy, 4, 1–16, doi: 10.1063/1.4769201, 2012.

515   NWTC 135-m Tower Data: https://nwtc.nrel.gov/MetData, last access: 18 May 2016.

Pauliac, R.: WINDCUBE user's manual, 2009.

Poulos, G.S., Bossert, J.E., Pielke, R.A., and McKee, T.B.: The interaction of katabatic flow and mountain waves I: observations and idealized simulations, J. Atmos. Sci., 57, 1919–1936, 2000.

Poulos, G.S., Bossert, J.E., Pielke, R.A., and McKee, T.B.: The interaction of katabatic flow and mountain waves II:
520   case study analysis and conceptual model, J. Atmos. Sci., 64, 1857–1879, 2007.

Rareshide, E., Tindal, A., Johnson, C., Graves, A.M., Simpson, E., Bleeg, J., Harris, T., and Schoborg, D.: Effects of complex wind regimes on turbine performance, AWEA Windpower 2009 meeting, Chicago, Ill., 2009.

Rhodes, M.E., and Lundquist, J.K.: The effect of wind-turbine wakes on summertime US Midwest atmospheric wind profiles as observed with ground-based Doppler LIDAR, Boundary-Layer Meteorol. 149, 85–103,
525   doi:10.1007/s10546-013-9834-x, 2013.

Rinker, J.M., Gavin, H.P., Clifton, A., Veers, P.S., and Kilcher, L.F.: Temporal coherence: a model for non-stationarity in natural and simulated wind records, Boundary-Layer Meteorol., 159, 373–389, doi: 10.1007/s10546-015-0121-x, 2016.

Smith, B., Link, H., Randall, G., and McCoy, T.: Applicability of Nacelle Anemometer Measurements for Use in
530   Turbine Power Performance Tests, AWEA Windpower, Portland, OR, 2002.

Stull, R.B.: An Introduction to Boundary Layer Meteorology, Kluwer Academic Publishers, Netherlands, 1988.

Sumner, J., and Masson, C.: Influence of atmospheric stability on wind turbine power performance curves, J. Sol. Energ.-T ASME, 128, 531–538, doi:10.1115/1.2347714, 2006.

van den Berg, G.P.: Wind turbine power and sound in relation to atmospheric stability, Wind Energy, 11, 151–169, 2008.

Vanderwende, B., and Lundquist, J.K.: The modification of wind turbine performance by statistically distinct atmospheric regimes, Environ. Res. Lett., 7, 1–7, doi:10.1088/1748-9326/7/3/034035, 2012.

Wagenaar, J.W., and Eecen, P.J.: Dependence of power performance on atmospheric conditions and possible corrections, European Wind Energy Association (EWEA) 2011 conference, Brussels, Belgium, 2011. http://www.ecn.nl/docs/library/report/2011/m11033.pdf, last access: 9 May 2016.

Wagner, R., Antoniou, I., Pedersen, S., Courtney, M., and Jorgensen, H.: The influence of the wind speed profile on wind turbine performance measurements, Wind Energy, 12, 348–362, doi:10.1002/we.297, 2009.

Walton, R.A., Takle, E.S., and Gallus Jr., W.A.: Characteristics of 50–200 m winds and temperatures derived from an Iowa tall-tower network, J. Appl. Meteorol. Clim., 53, 2387–2393, doi:10.1175/JAMC-D-13-0340.1, 2014.

Wharton, S., and Lundquist, J.K.: Atmospheric stability affects wind turbine power collection, Environ. Res. Lett., 7, 1–9, doi:10.1088/1748-9326/7/014005, 2012a.

Wharton, S. and Lundquist, J.K.: Assessing atmospheric stability and its impacts on rotor-disk wind characteristics at an onshore wind farm, Wind Energy, 15, 525–546, doi:10.1002/we.483, 2012b.

Zahle, F., and Sørensen, N.N.: Characterization of the unsteady flow in the nacelle region of a modern wind turbine, Wind Energy, 13, 271-283, doi: 10.1002/we.418, 2011.

Table 1. 135-m met tower instrument information

Type	Instrument	Mounting Heights (m)	Accuracy
Cup anemometer	Met One SS-201	3, 10, 38, 87, 122	0.5 m s^{-1}
Cup anemometer	Thies 4.3351.10.0000	30, 55, 80, 105, 130	0.2 m s^{-1}
Wind vane	Met One SD-201	3, 10, 38, 87, 122	3.6°
Air temperature sensor	Met One T-200A platinum RTD	3, 38, 87	0.1°C
Differential temperature sensor	Met One T-200A	38, 87, 122	0.1°C
Sonic anemometer	ATI 'K' type	15, 41, 61, 74, 100, 119	0.01 m s^{-1}
Boom triaxial acceleration sensor	Summit 34201A	15, 41, 61, 74, 100, 119	
Sonic temperature	ATI 'K' type	15, 41, 61, 74, 100, 119	0.1°C
Barometric pressure sensor	AIR AB-2AX	3	
Dewpoint temperature sensor	Therm-x 9400ASTD	3, 38, 87, 122	
Precipitation sensor	Vaisala DRD11A	3	

Table 2. Defined stability regimes

Stability class	R_B	L (m)	α
Unstable conditions	$R_B < -0.03$	$-1{,}000 < L \leq 0$	$\alpha < 0.11$
Neutral conditions	$-0.03 < R_B < 0.03$	$|L| \geq 1{,}000$	$0.11 < \alpha < 0.17$
Stable conditions	$R_B > 0.03$	$0 \leq L < 1{,}000$	$\alpha > 0.17$

Table 3. Defined turbulence regimes

Turbulence regime	TI (%)	TKE ($m^2\ s^{-2}$)
High turbulence	TI > 20	TKE > 6.5~~5~~
Medium turbulence	15 < TI < 20	3.0~~2.5~~ < TKE < 6.5~~5~~
Low turbulence	TI < 15	TKE < 3.0~~2.5~~

Table 4. Weibull parameters for the case of no stability or turbulence filter as well as for each turbulence and stability class.

	Scale parameter	Shape parameter	Mean
No filter	10.04	2.63	8.90
low TI regime	10.83	2.59	9.60
med TI regime	10.81	2.90	9.63
high TI regime	8.52	2.81	7.57
low R_B regime	10.12	3.09	9.05
med R_B regime	13.29	3.45	11.96
high R_B regime	7.64	3.10	6.83

Table 4~~5~~. AEP in megawatt-hours/year calculated for different atmospheric and turbulence regimes using a Weibull distribution with a scale and shape parameters associated with the corresponding wind speed distribution~~with a scale factor of 10.13 m s^{-1} and a shape factor of 2.62~~.

	~~No filter~~	~~TI filter~~	~~α filter~~	~~R_B filter~~
~~AEP (MWh/y)~~	~~7,546.5~~	~~7,384.1~~	~~7,343.9~~	~~6,780.2~~

	No filter	TI filter	R_B filter
AEP using tower data	7,479.3	7,409.6	7,278.7
AEP using nacelle data	7,430.6	7,388.9	7,266.7

Table ~~5~~6. AEP in percentage calculated for different filter regimes using a Weibull distribution ~~with a scale factor and a shape factor representative of the corresponding wind speed distribution.~~ with a scale factor of 10.13 m s^{-1} and a shape factor of 2.62. Medium regime is set at 100 % and low and high regimes are percentages compared to the medium regime. Boxes with the highest value within that row are italicized.

~~Filter~~	~~Low regime~~	~~Medium regime~~	~~High regime~~
~~TI~~	~~88.11~~	~~*100.00*~~	~~84.63~~
~~α~~	~~101.18~~	~~100.00~~	~~*102.20*~~
~~R_B~~	~~*147.80*~~	~~100.00~~	~~118.89~~

Filter	Low regime	Medium regime	High regime
TI using tower data	85.03	*100.00*	68.20
R_B using tower data	*116.28*	100.00	71.33
TI using nacelle data	84.76	*100.00*	68.32
R_B using nacelle data	*115.86*	100.00	70.52
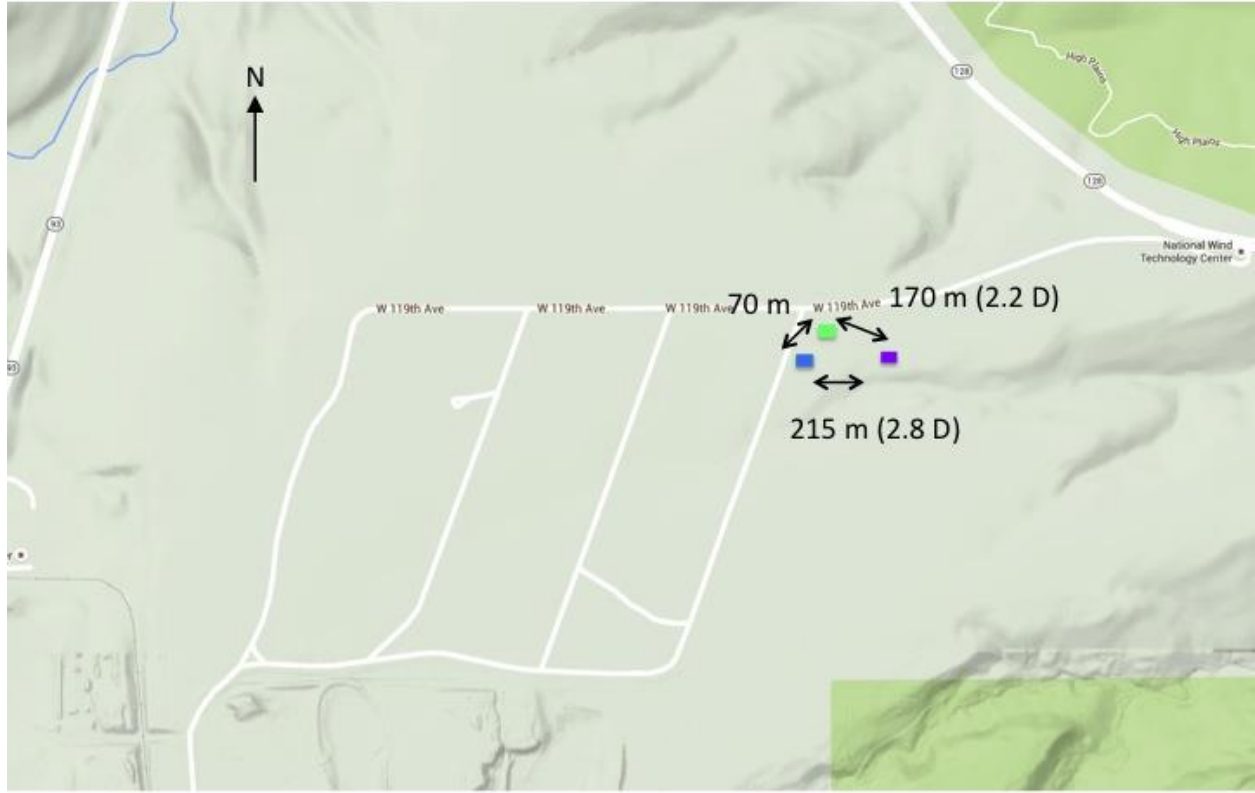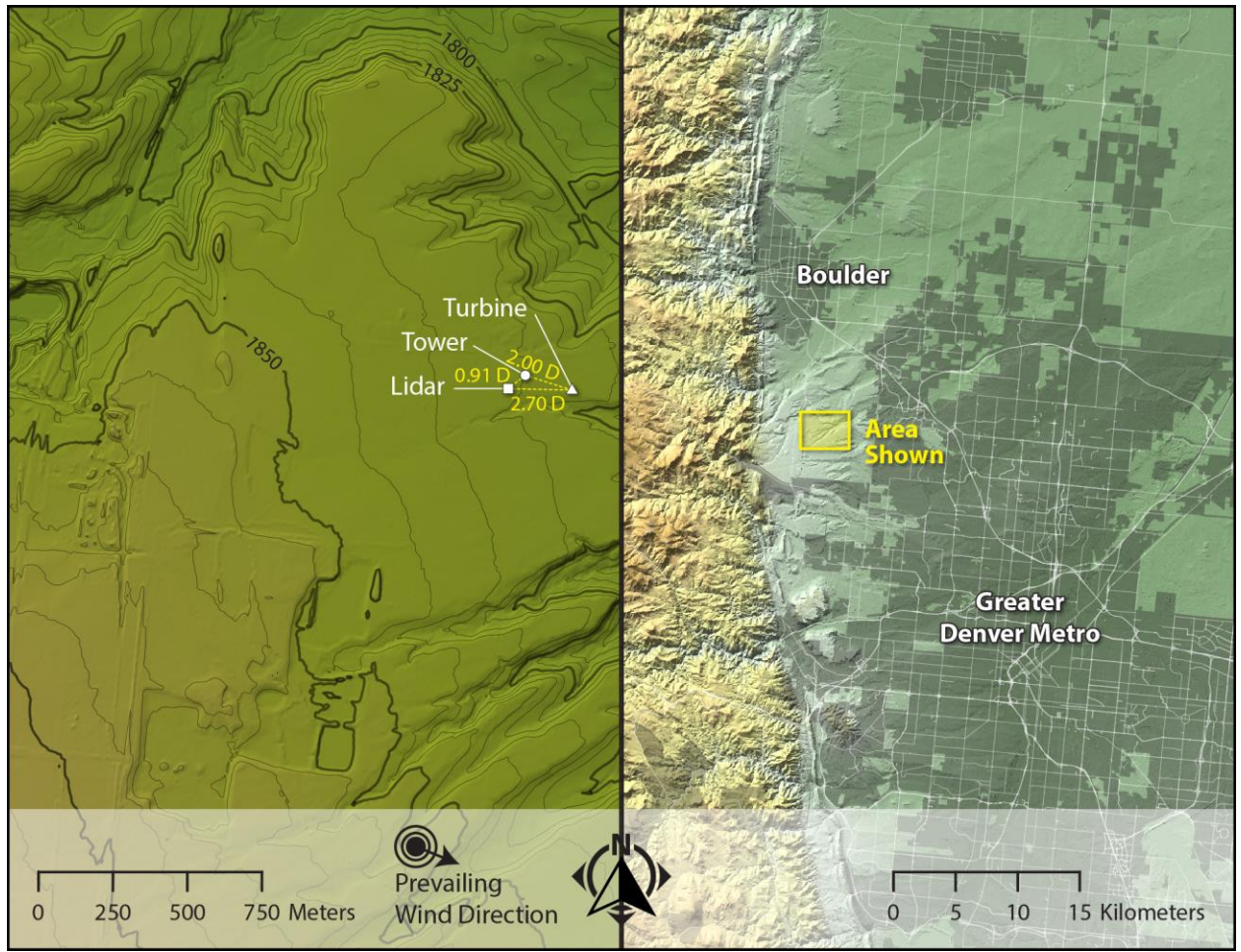
Figure 1. ~~Top: Google Maps image~~Left: Local map of the NWTC with instrument locations and topographic contours in meters above sea level. Right: The regional setting of the NWTC between the Greater Denver Metro area and Boulder, with the Front Range of the Rocky Mountains shown in the higher topography west of the site. ~~The green rectangle represents the location of the met tower, the purple rectangle represents the location of the turbine, and the blue rectangle represents the location of the lidar. Map Data © 2016 Google.~~
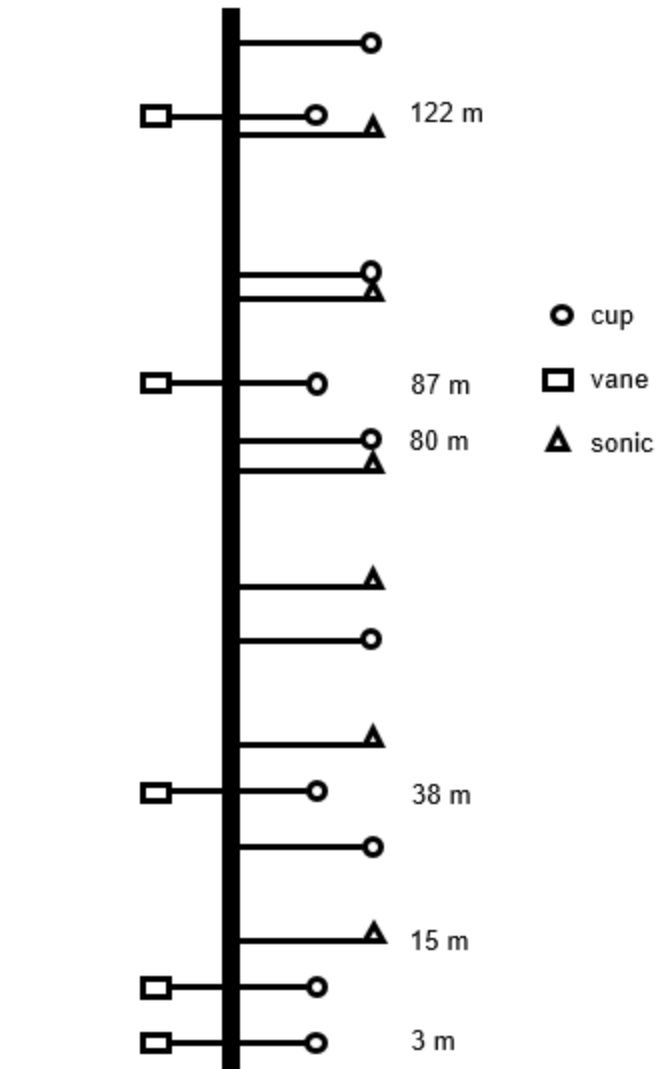
Figure 2. 135‑m meteorological tower configuration with some. A few key heights are labeled. This tower variesis slightly different from the M4 tower described in Clifton et al. (2013), but data are available online (NWTC, 2016).
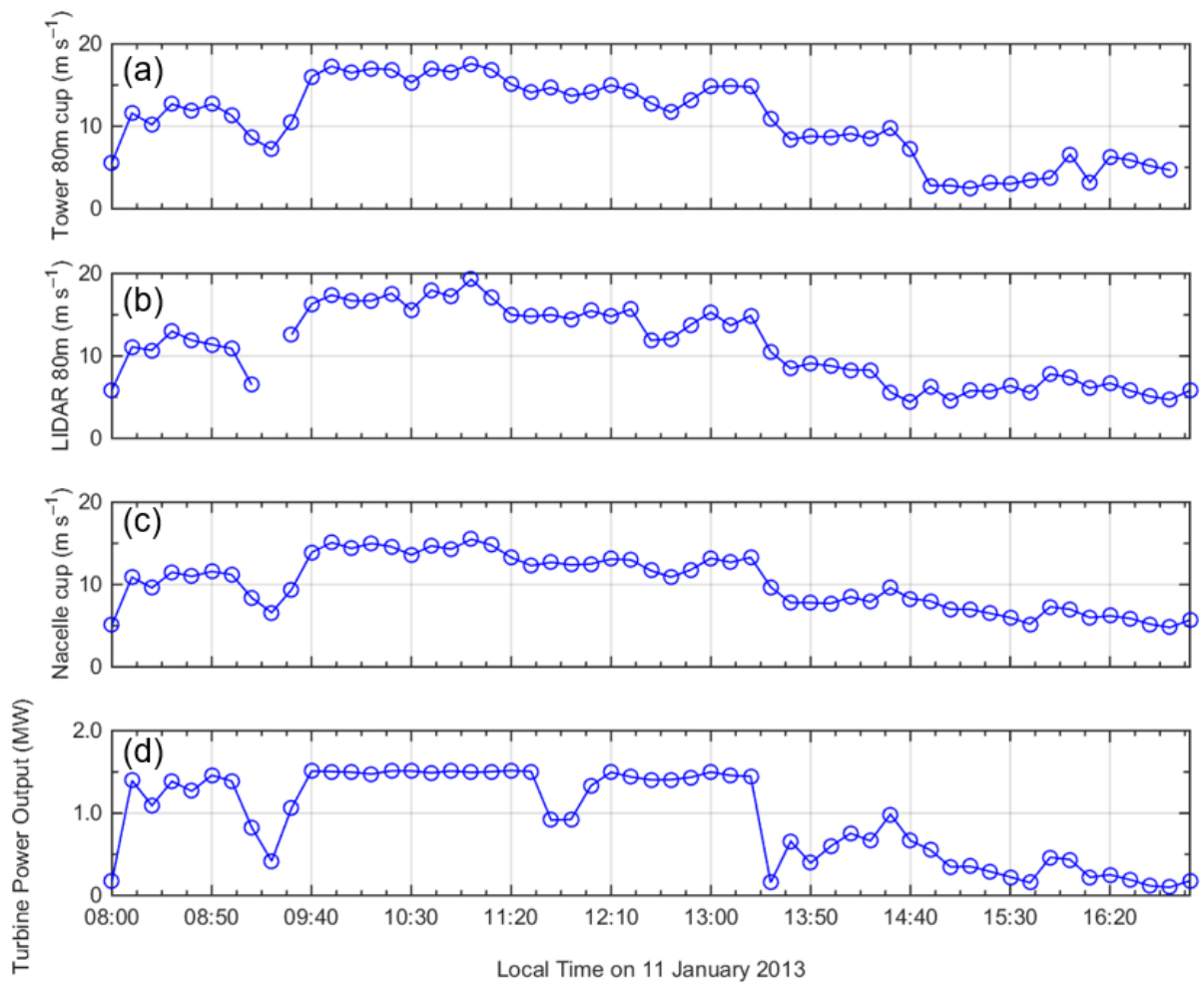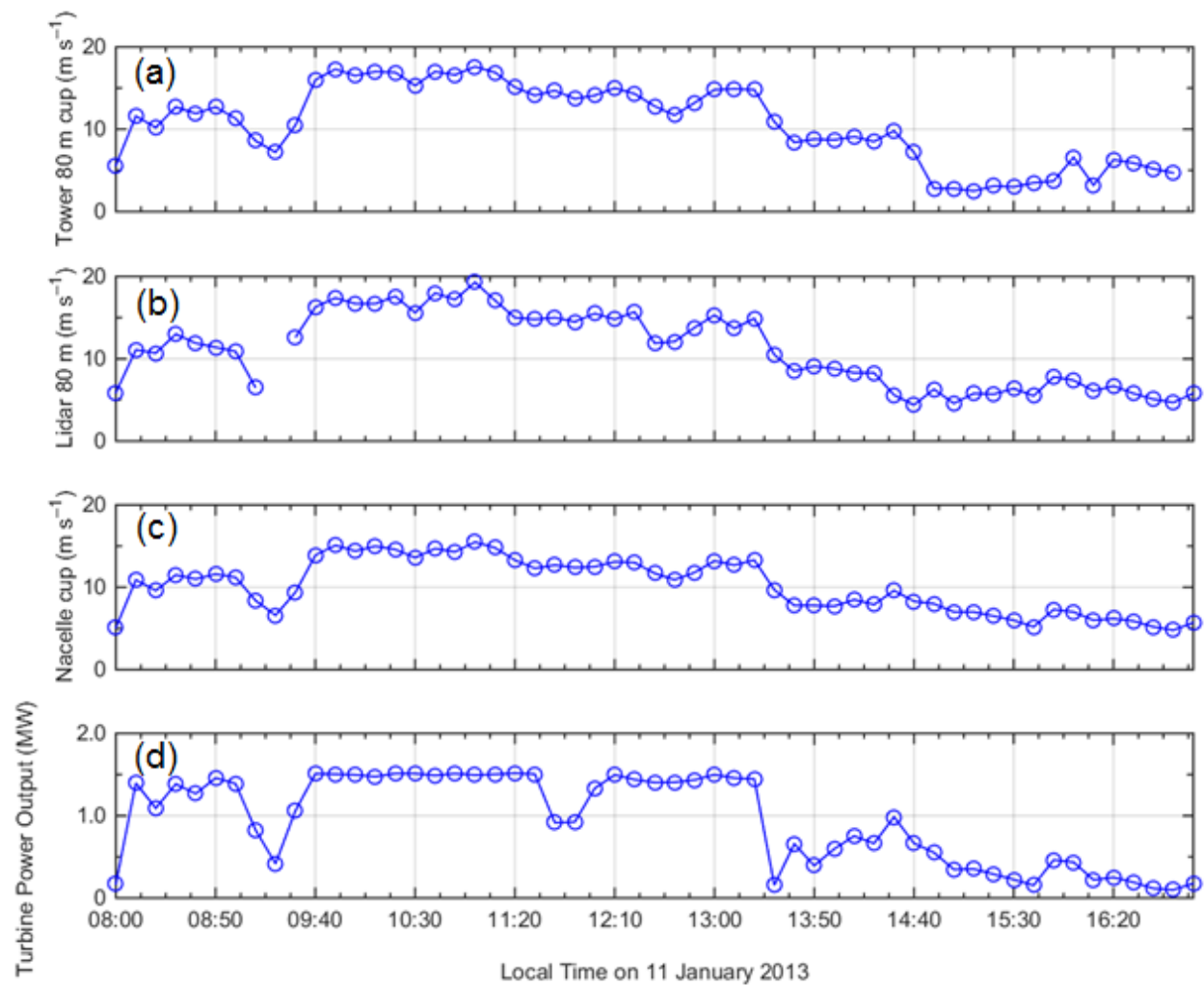
Figure 3. Time series from 11 January 2013 from 08:00 to 17:00 Mountain Standard Time (MST): (a) is a time series of 80-m wind speeds measured by the cup on the tower; (b) is a time series of 80-m wind speeds measured by the lidar; (c) is a time series of the hub--height wind speeds measured by the cup anemometer on the nacelle; and (d) is a time series of the power output from the turbine.
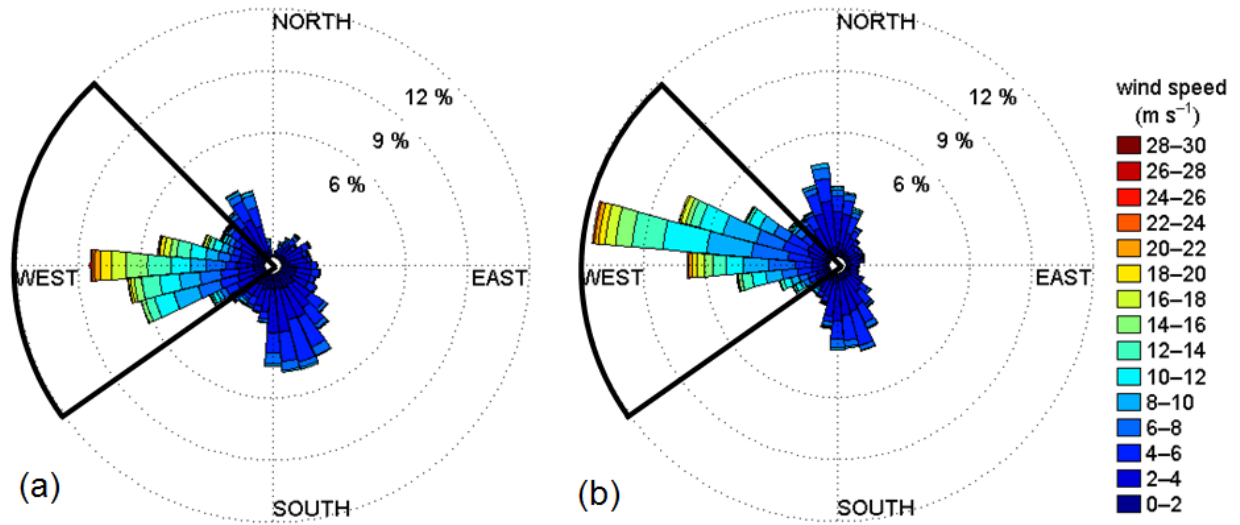
Figure 4. Wind roses for (a) lidar 80-m altitude and (b) met tower 87-m altitude, the~~(altitude~~ closest to hub-height with both a cup and vane~~)~~. Wind bins are 2 m s⁻¹ and wind directions bins are 10°. The b~~B~~lack outline highlights the chosen wind direction sector.
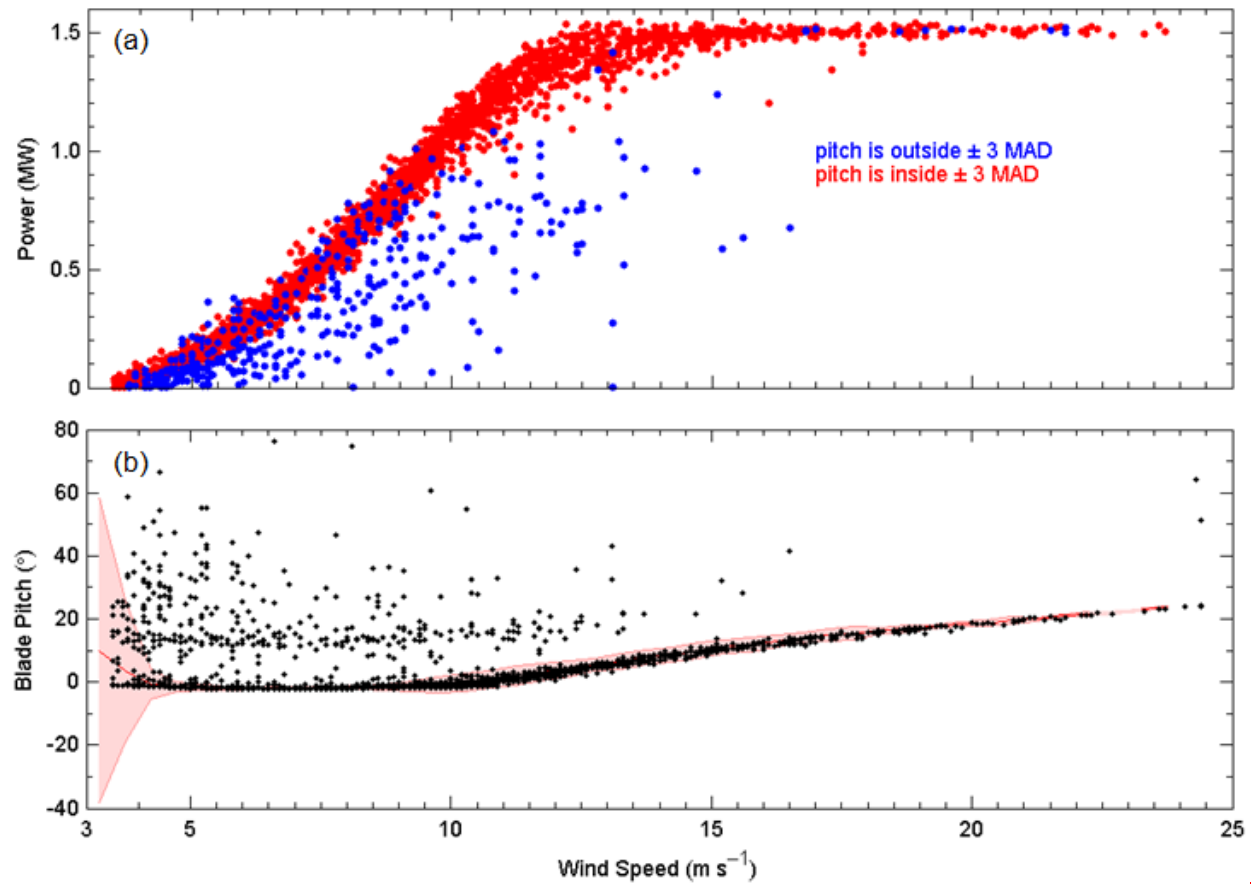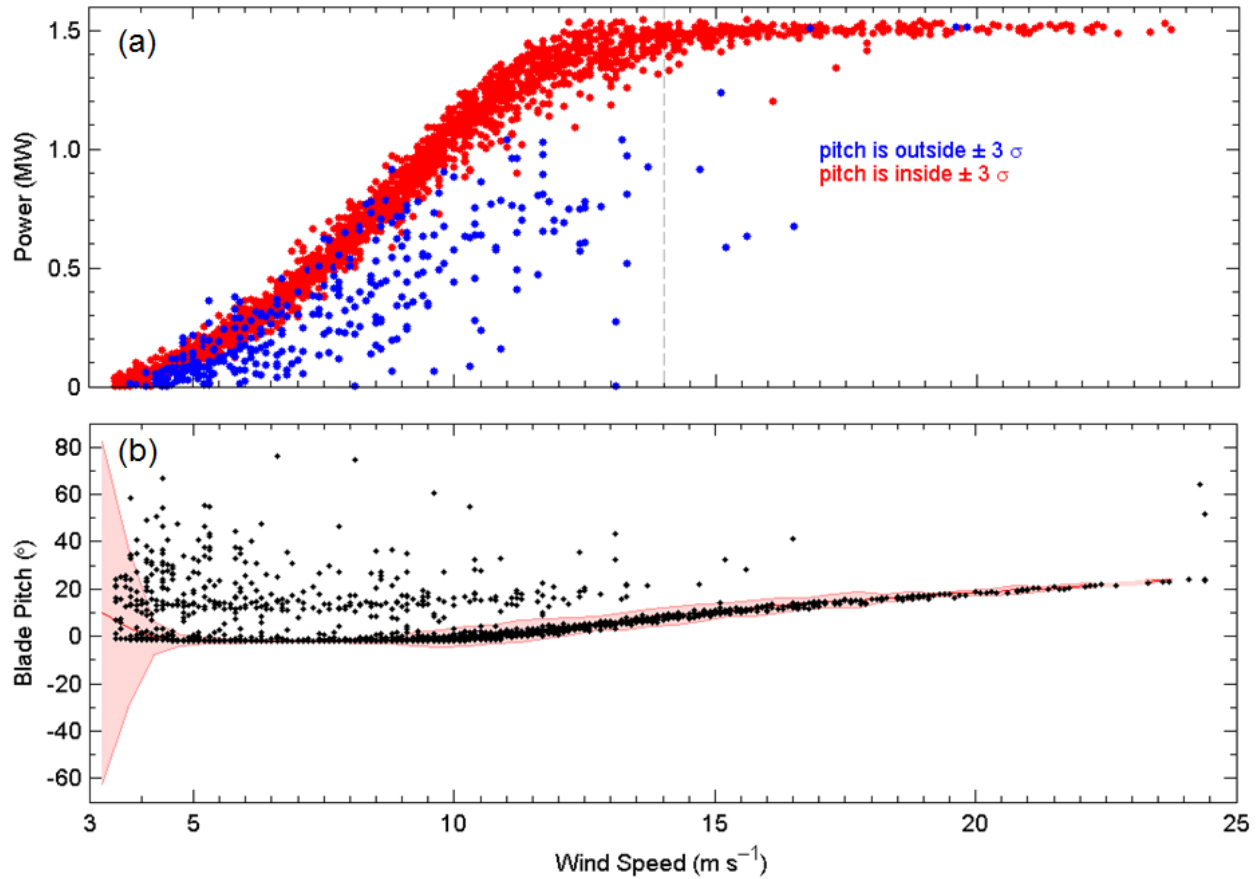
Figure 5. (a) Scatter power curve based on~~using~~ the tower 80-m wind speed. ~~The b~~Blue dots~~scatter~~ shows~~the~~ points that are outside of the median absolute devation (MAD) envelope in (b) and the red ~~scatter~~ dots ~~shows the~~ represent points ~~that are~~ within the MAD envelope in (b). The grey dashed line marks rated speed; (b) blade pitch angle from a single blade versus tower 80-m wind speed. Red envelope represents $\pm$ 4.5~~3~~ MAD of the blade pitch angle within wind speed bins 0.5 m s^{-1} wide.
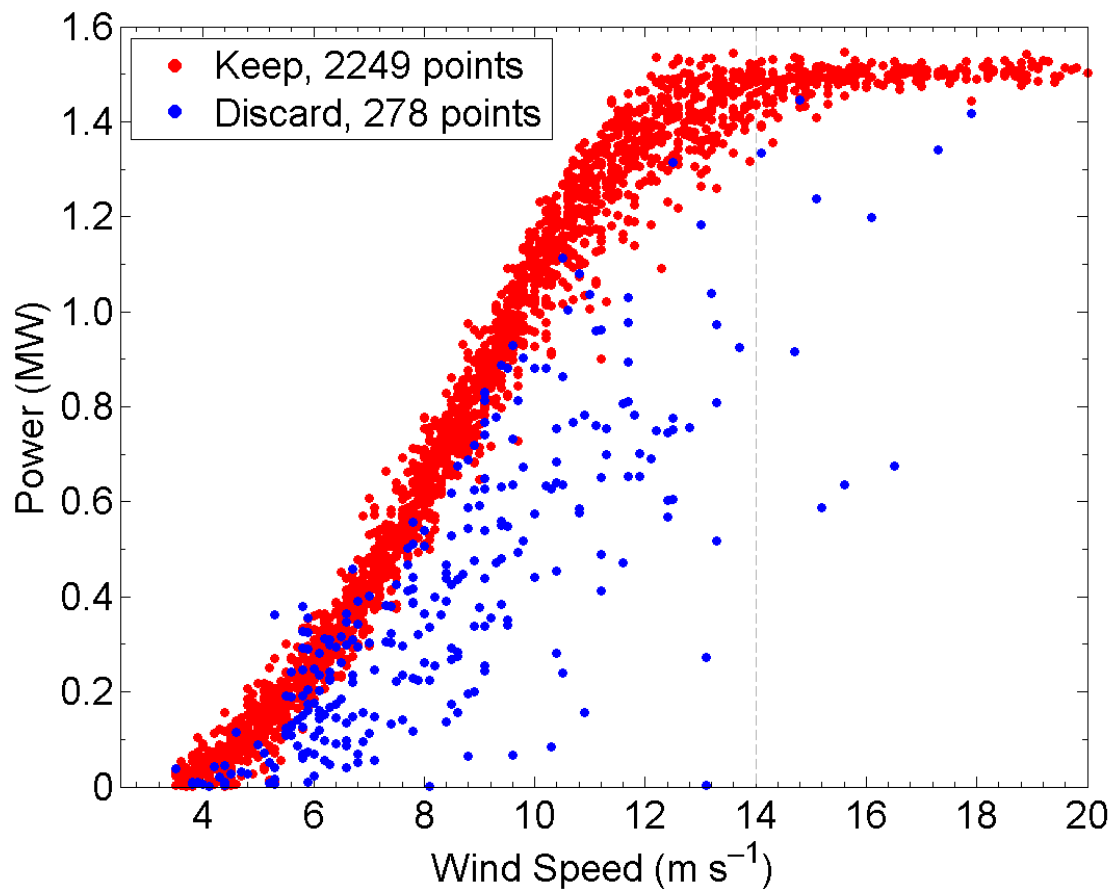
Figure 6. Scatter power curve using the tower 80-m wind speed. Blue dots show points filtered out using turbine control parameters described in Sect. 3.3.2. Red dots show data points that pass this filtering process. The grey dashed line marks rated speed.
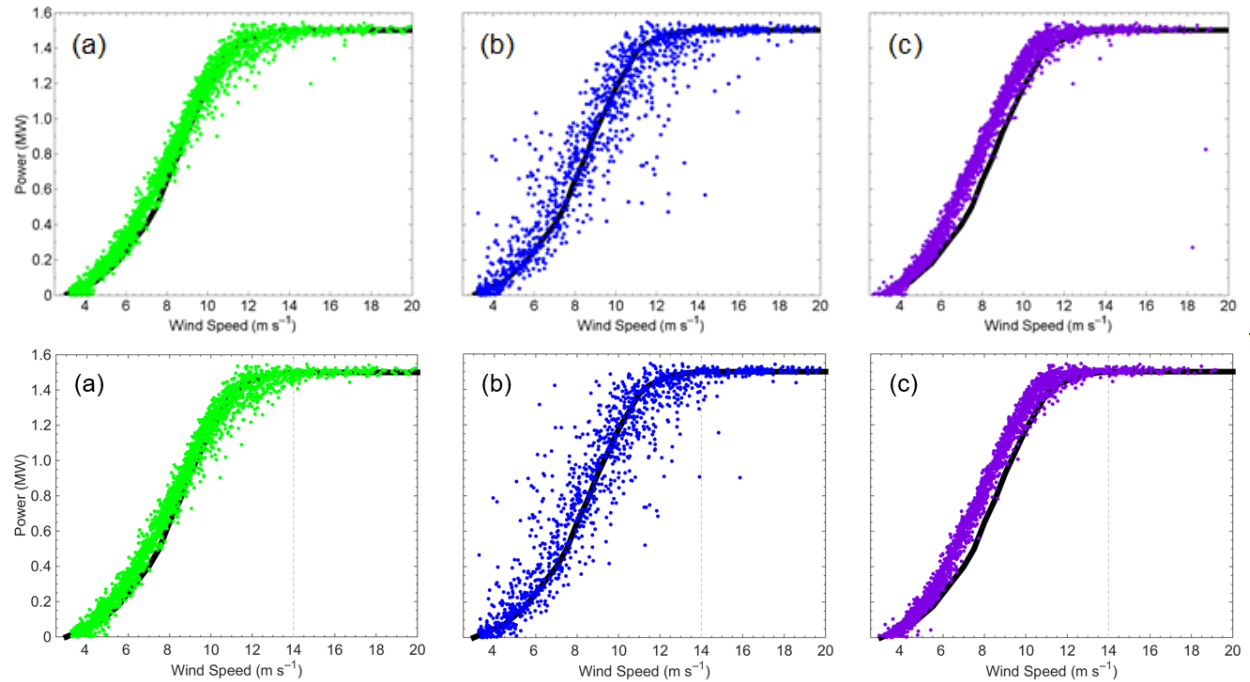
Figure 67. Power curves after filtering for wind speeds between 3.5 and 25 m s^{-1}, wind directions between 235°and 315°, and for normal turbine operation:blade pitch angle within ± 3 MAD: (a) turbine power production versus 80-m cup anemometer wind speed from the met tower; (b) turbine power production versus 80-m wind speed from the lidar; (c) turbine power production versus hub-height wind speed from the anemometer on the nacelle. The blackGrey line represents an approximation of the manufacturer power curve for the GE 1.5sle (GE Energy, 2009). Wind speed is normalized for density following IEC 61400-12-1 (2015). The grey dashed line marks rated speed.
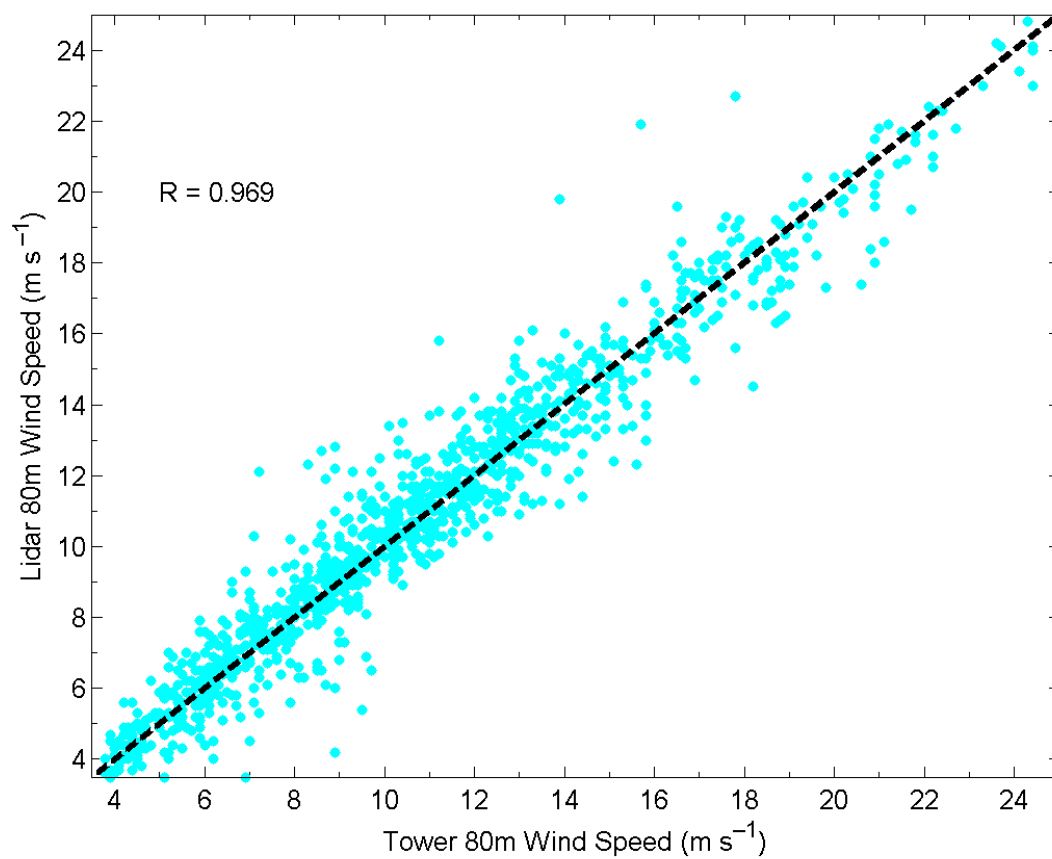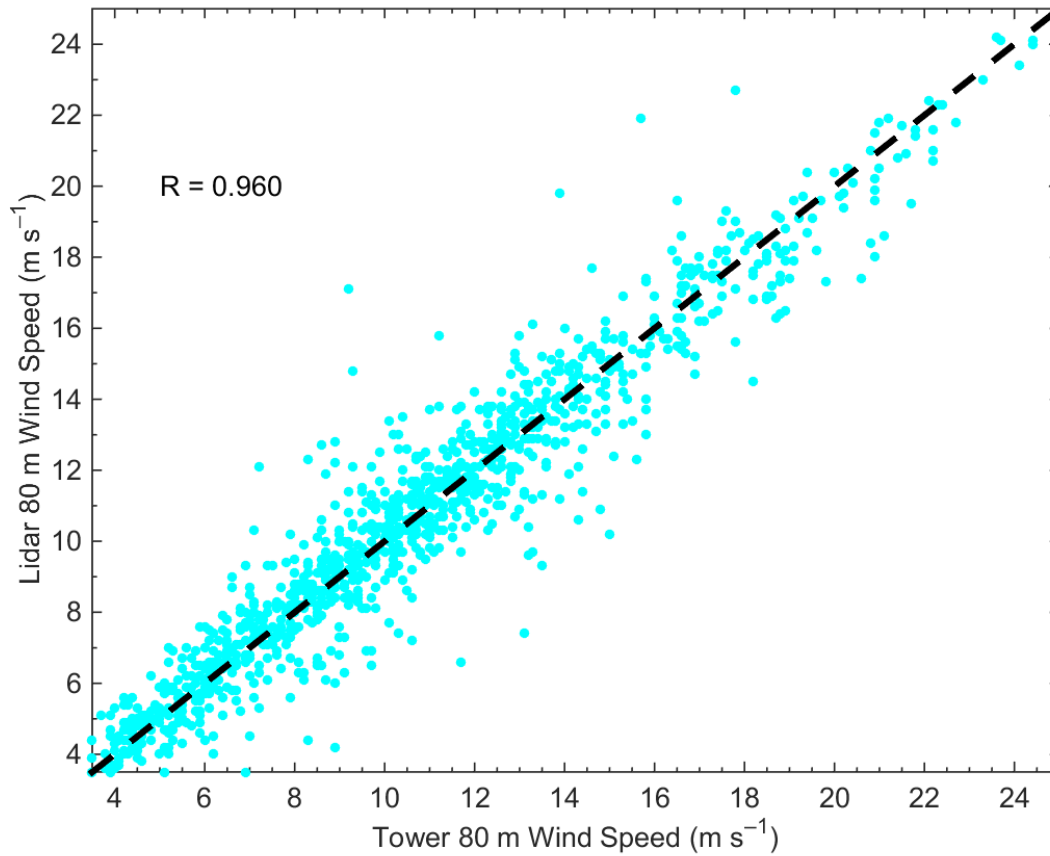
Figure 78. Lidar 80-m wind speeds compared to tower 80-m wind speeds filtered for wind speeds between 3.5 and 25.0 m s⁻¹, wind directions between 235° and 315°, and for normal turbine operation blade pitch angle within ± 3 MAD. The bBlack dashed line represents a 1:1 relationship.
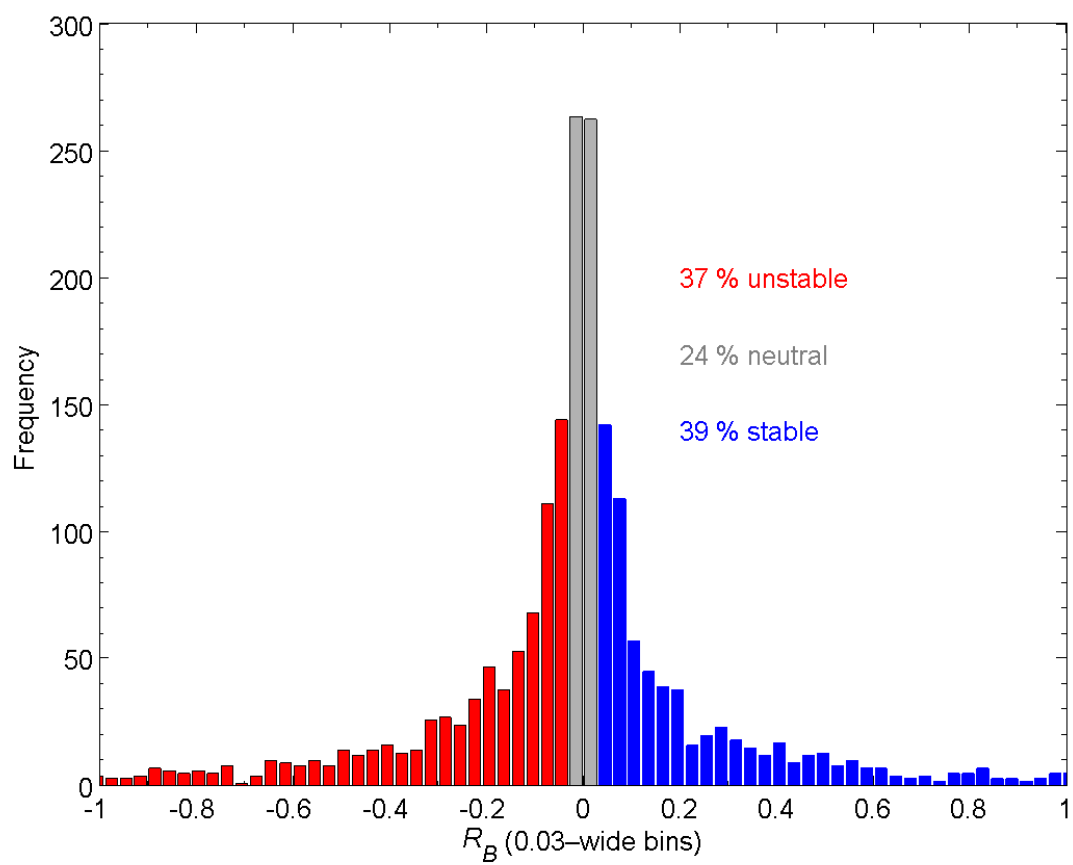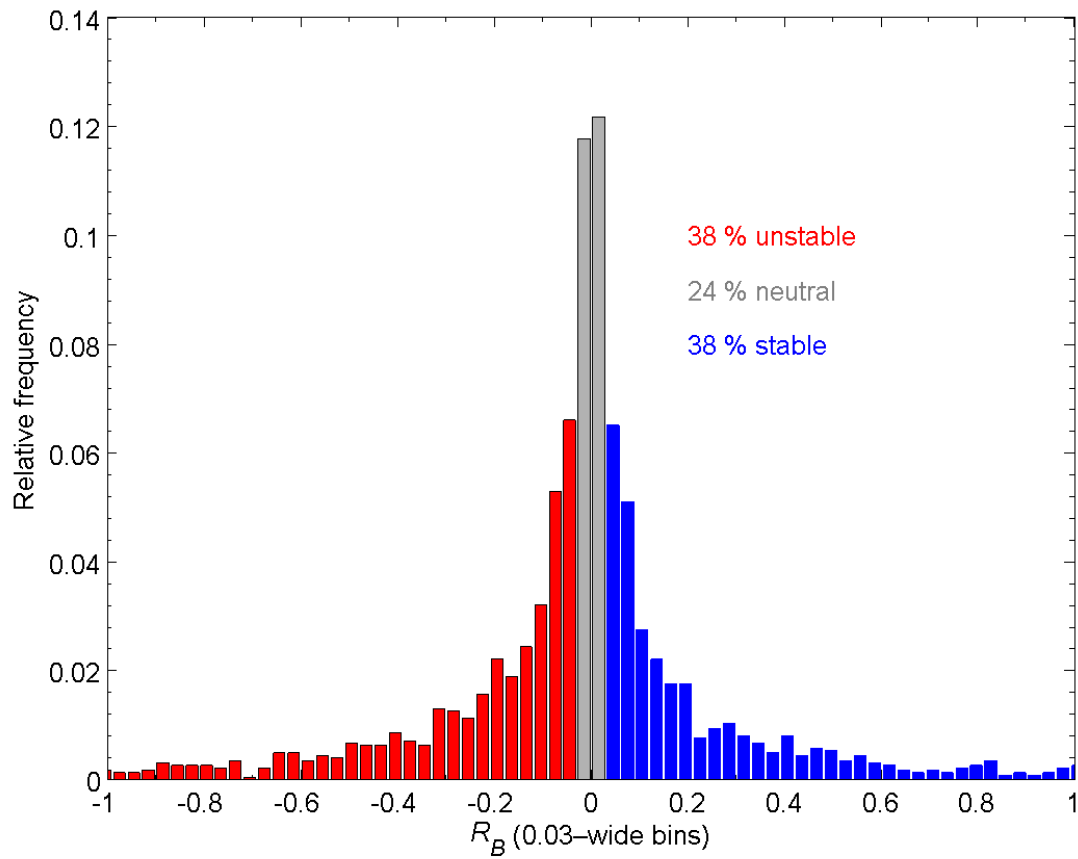
Figure ~~8~~9. R_B distribution using thresholds in Table 2~~, i.~~ ~~I~~ncludi~~ng~~es data filtered for tower 80~~-~~m wind speeds between 3.5 and 25.0 m s^{-1}, 87~~-~~m wind directions between 235° and 315°, and ~~for normal turbine operation~~ ~~blade pitch angle within ± 3 MAD~~.
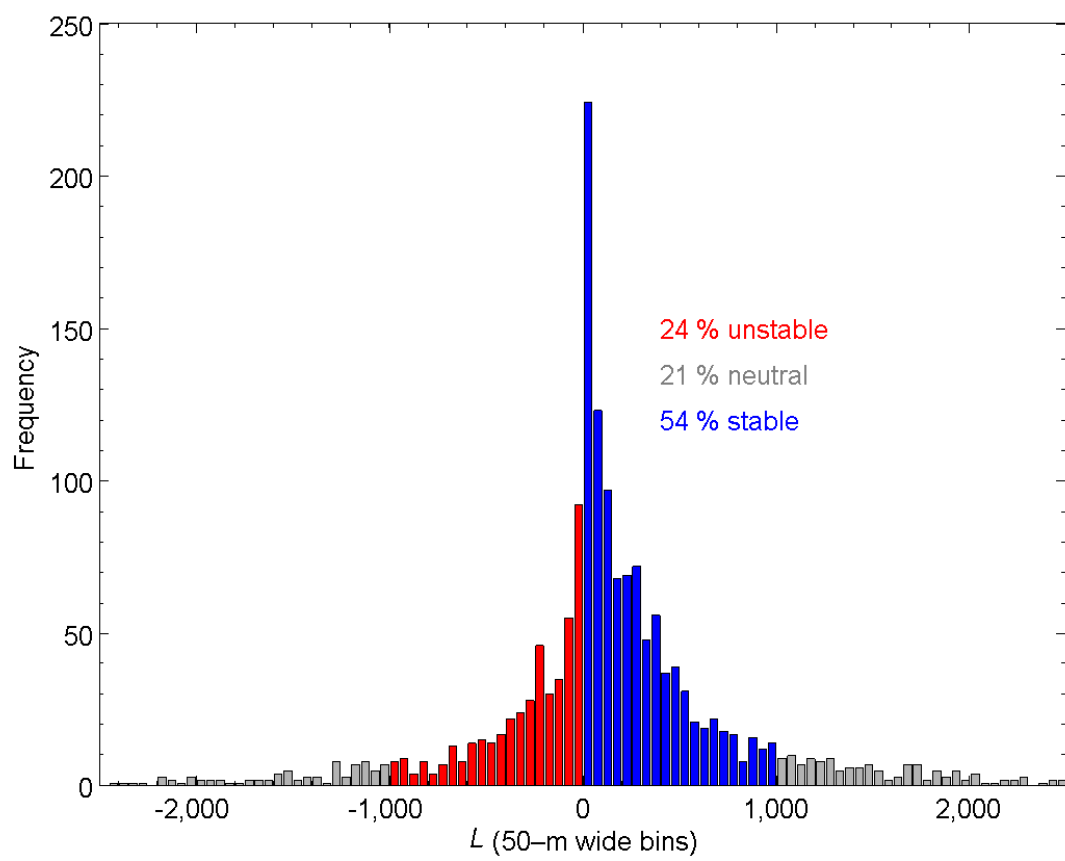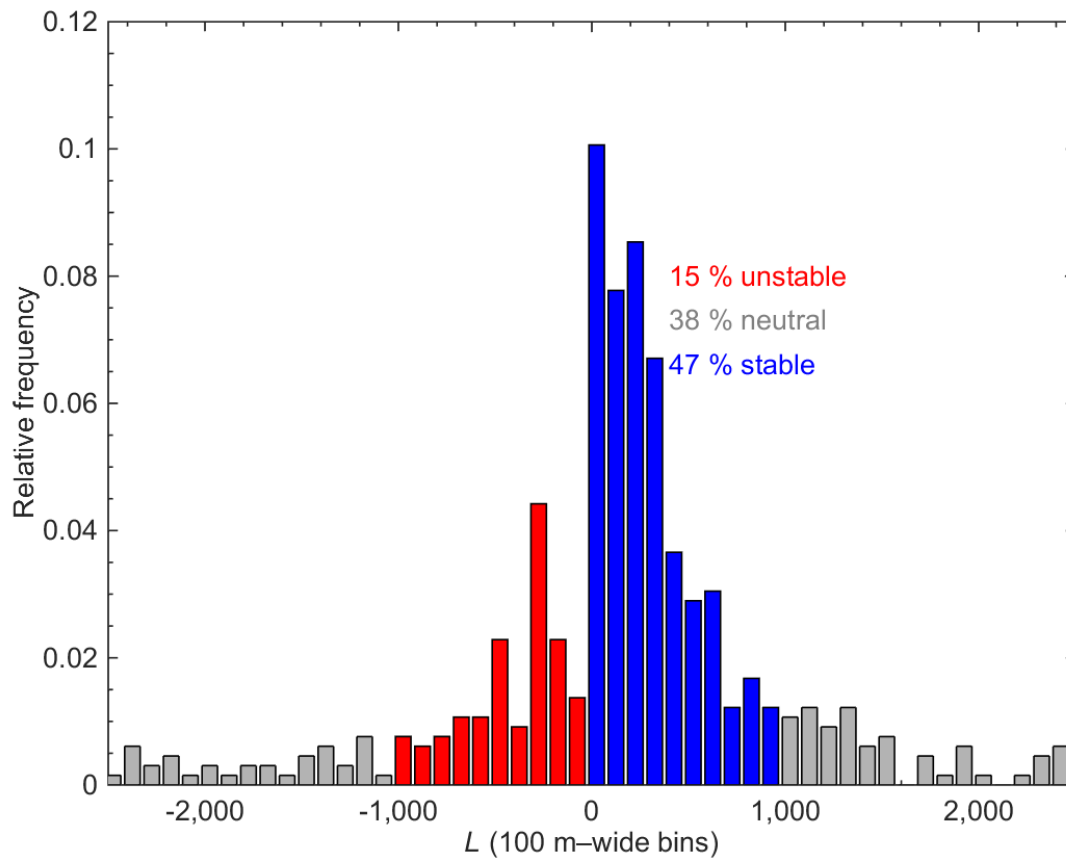
Figure 910. *L* distribution using thresholds in Table 2. Note that some neutral cases are outside of these axes. Includes data filtered for tower 80-m wind speeds between 3.5 and 25.0 m s⁻¹, 87-m wind directions between 235° and 315°, and for normal turbine operation.blade pitch angle within ± 3 MAD.
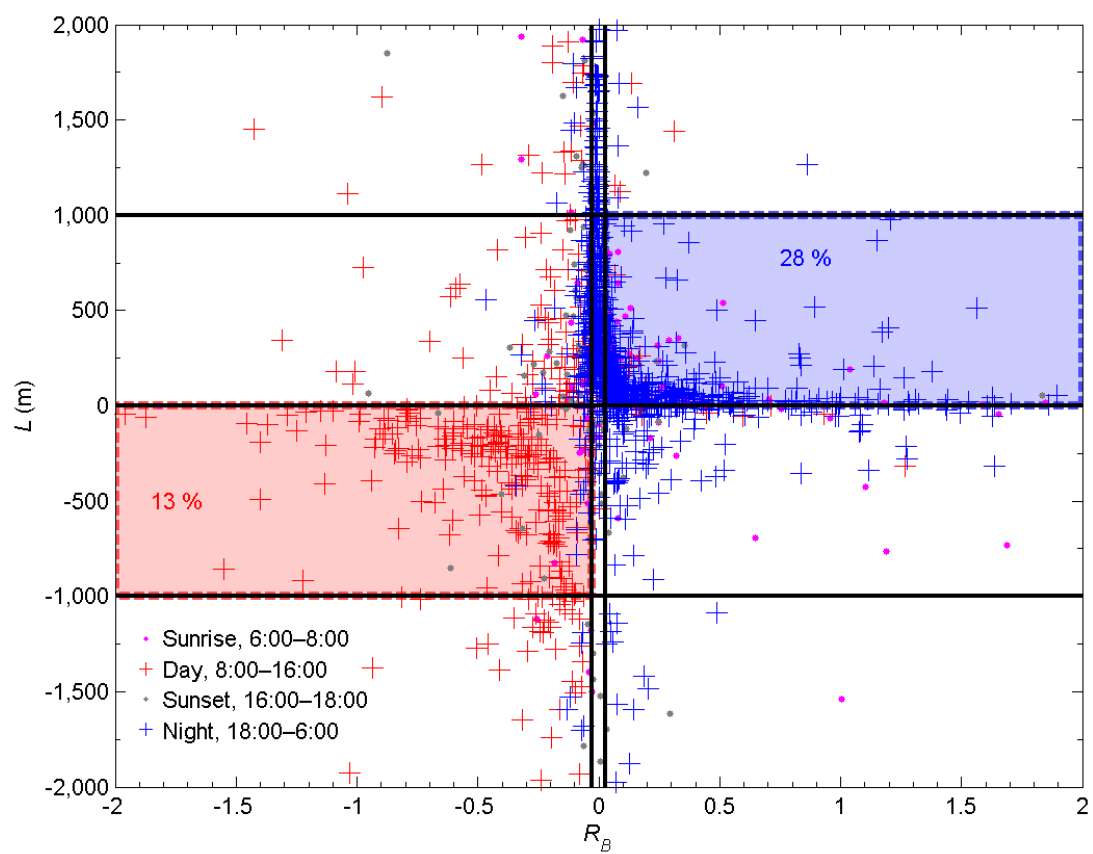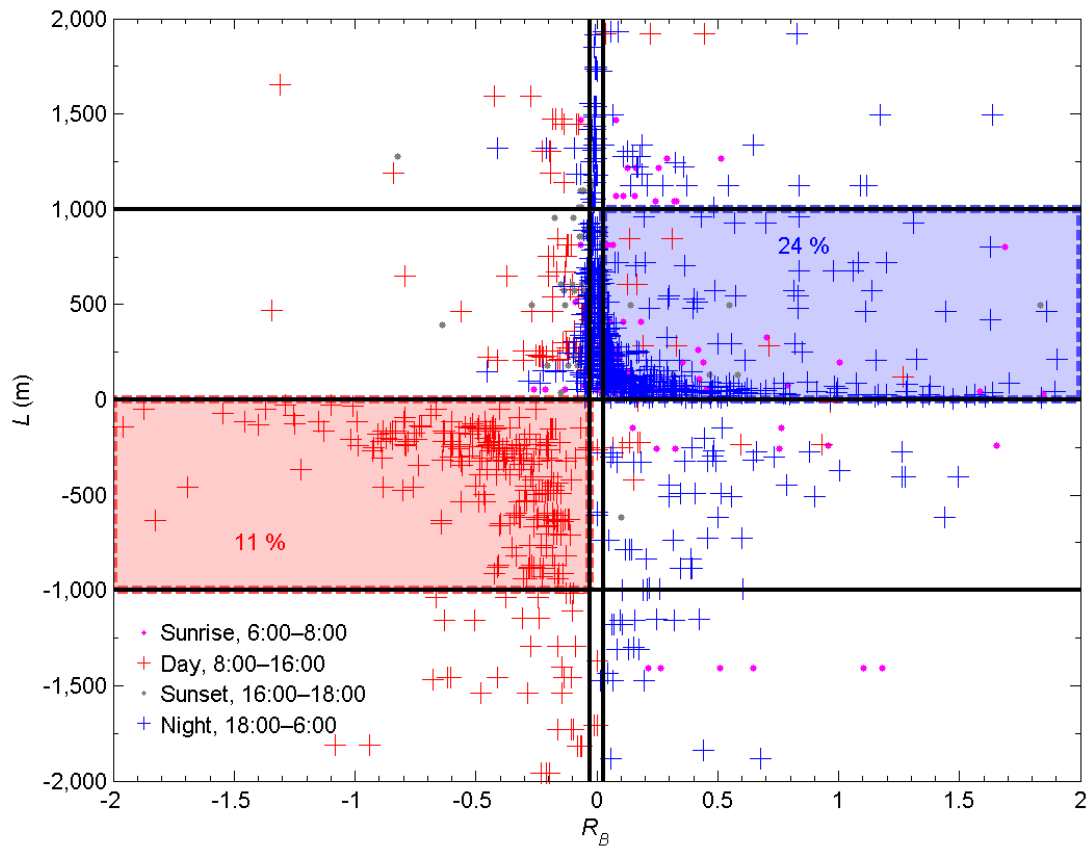
Figure ~~10~~11. L versus R_B. Blue box represents where both L and R_B agree on the stable conditions; percentage (24 %) represents the percentage of data points in this box. Red box represents where both L and R_B agree on the unstable conditions; percentage (11 %) represents the percentage of data points in this box. Includes data filtered for tower 80-m wind speeds between 3.5 and 25 m s^{-1}, 87-m wind directions between 235° and 315°, and for normal turbine operation ~~blade pitch angle within ± 3 MAD~~.
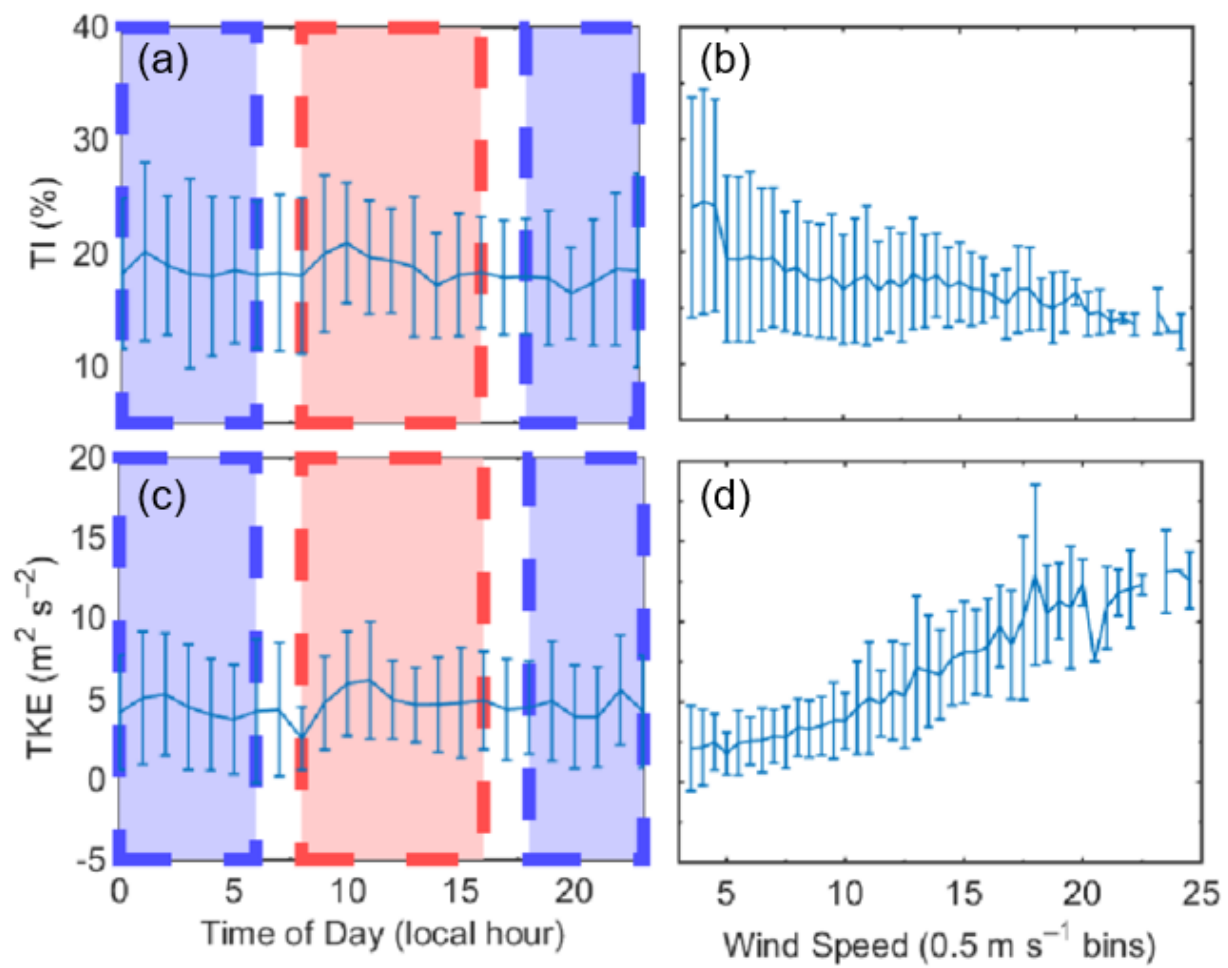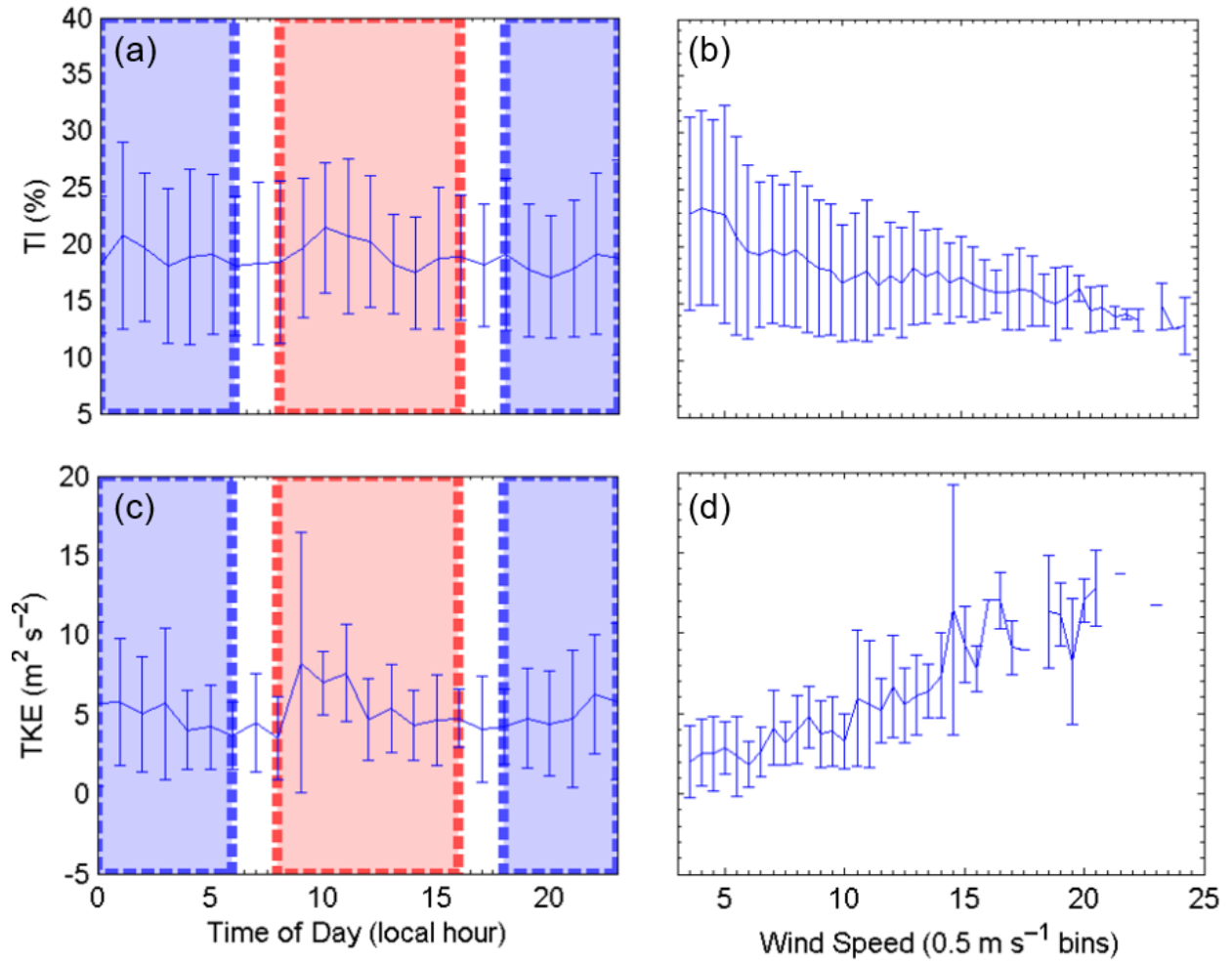
Figure ~~11~~12. TI (a) and TKE (c) calculated with near hub-­height tower measurements versus time of day, where hour 0 and hour 24 represent _local_ midnight. The blue line represents the mean TI in the corresponding hour and the error bar represents the standard deviation. The blue rectangle represents nighttime hours and the red rectangle represents daytime hours. Mean and standard deviation of TI (b) and TKE (d) calculated with near hub-­height tower measurements in each wind speed bin. Includes data filtered for tower 80-­m wind speeds between 3.5 and 25.0 m s^{-1}, 87-­m wind directions between 235° and 315°, and ~~for~~ _normal turbine operation_ ~~blade pitch angle within ± 3 MAD~~.
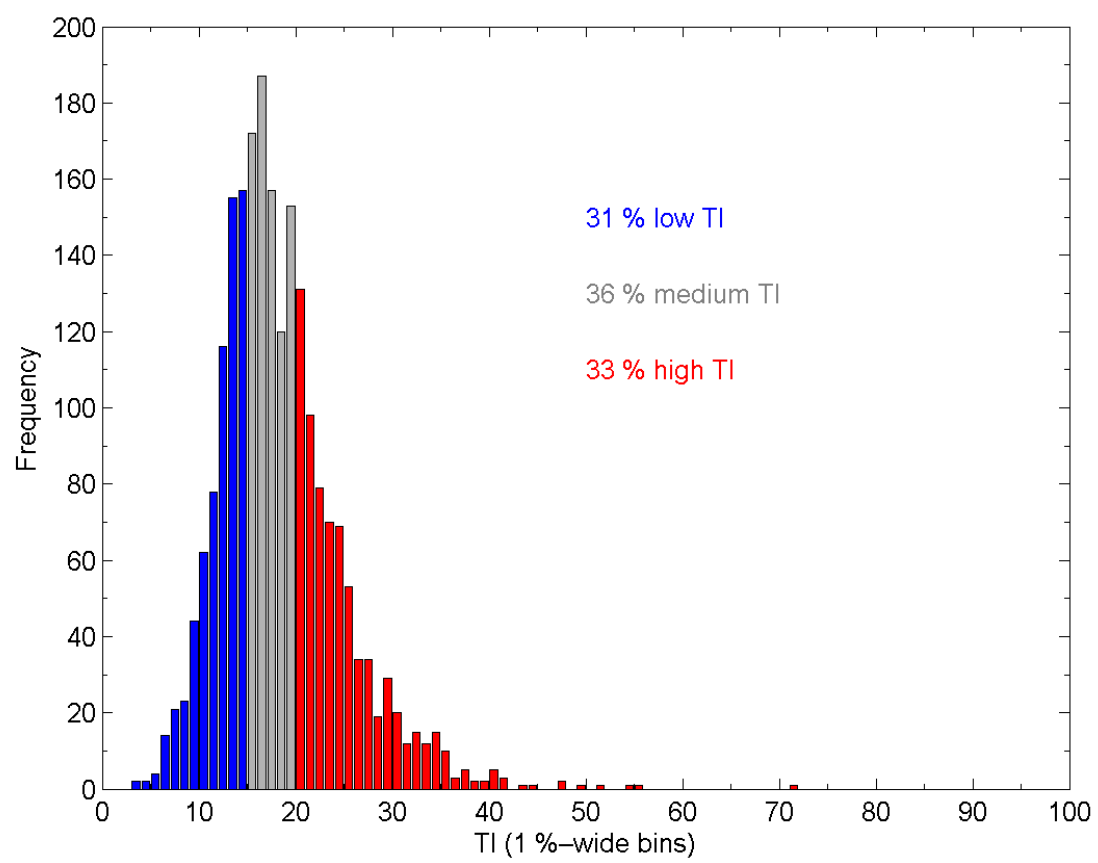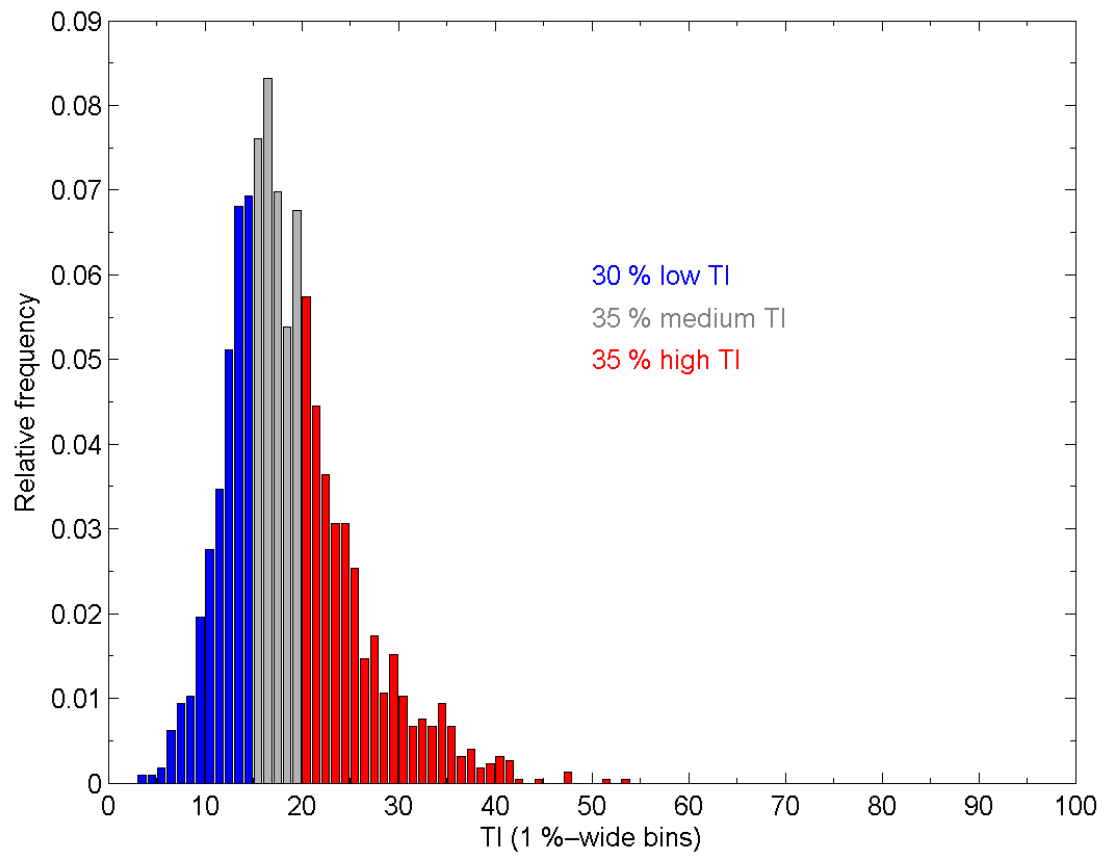
Figure ~~12~~13. TI distribution using thresholds in Table 3. Includes data filtered for tower 80-m wind speeds between 3.5 and

25 m s^{-1}, 87-m wind directions between 235° and 315°, and- for normal turbine operation ~~blade pitch angle within ± 3 MAD~~.
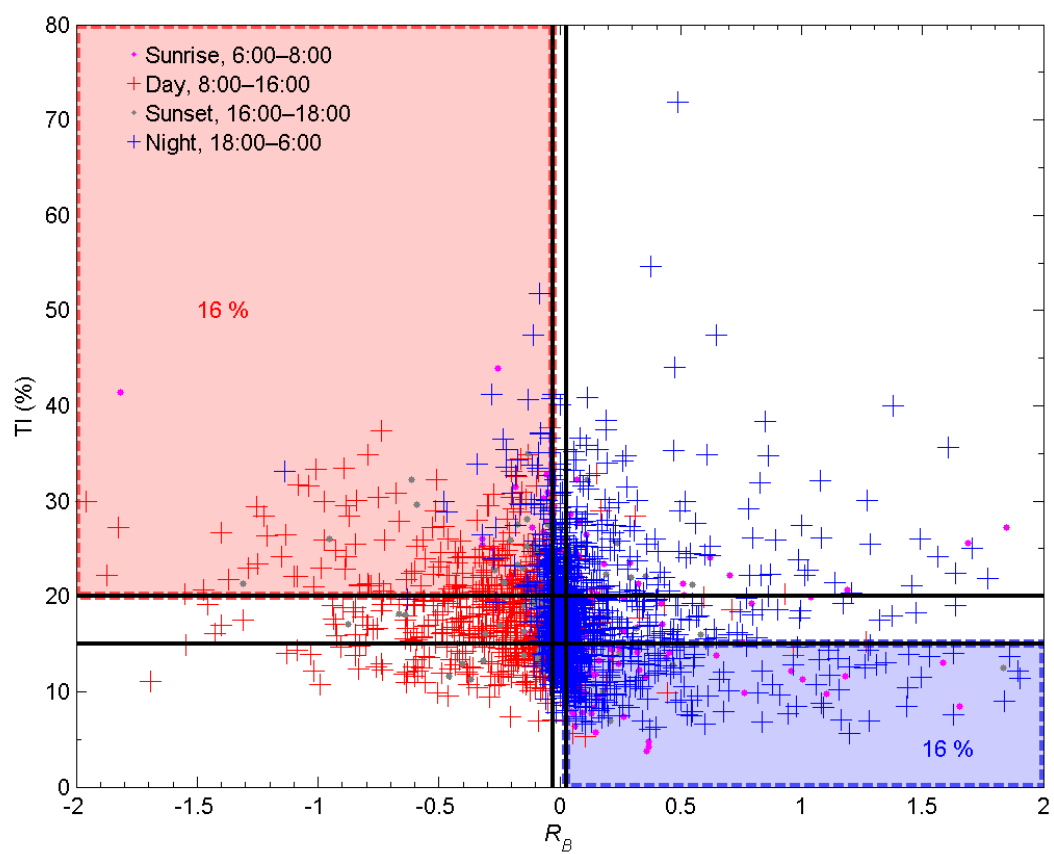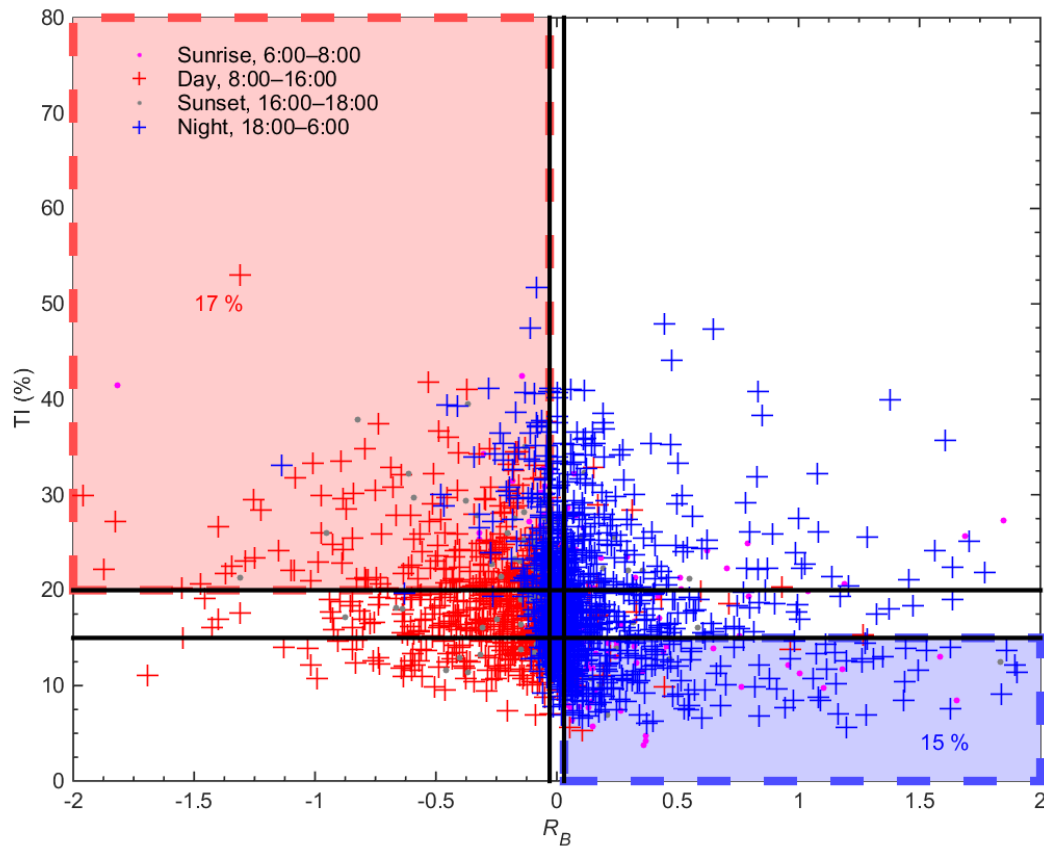
Figure ~~13~~14. TI versus R_B . Blue box represents where both TI and R_B agree on the stable conditions; percentage (15 %) represents the percentage of data points in this box. Red box represents where both TI and R_B agree on the unstable conditions; percentage (17 %) represents the percentage of data points in this box. Includes data filtered for tower 80-m wind speeds between 3.5 and 25 m s^{-1}, 87-m wind directions between 235° and 315°, and for normal turbine operation ~~blade pitch angle within ± 3 MAD~~.
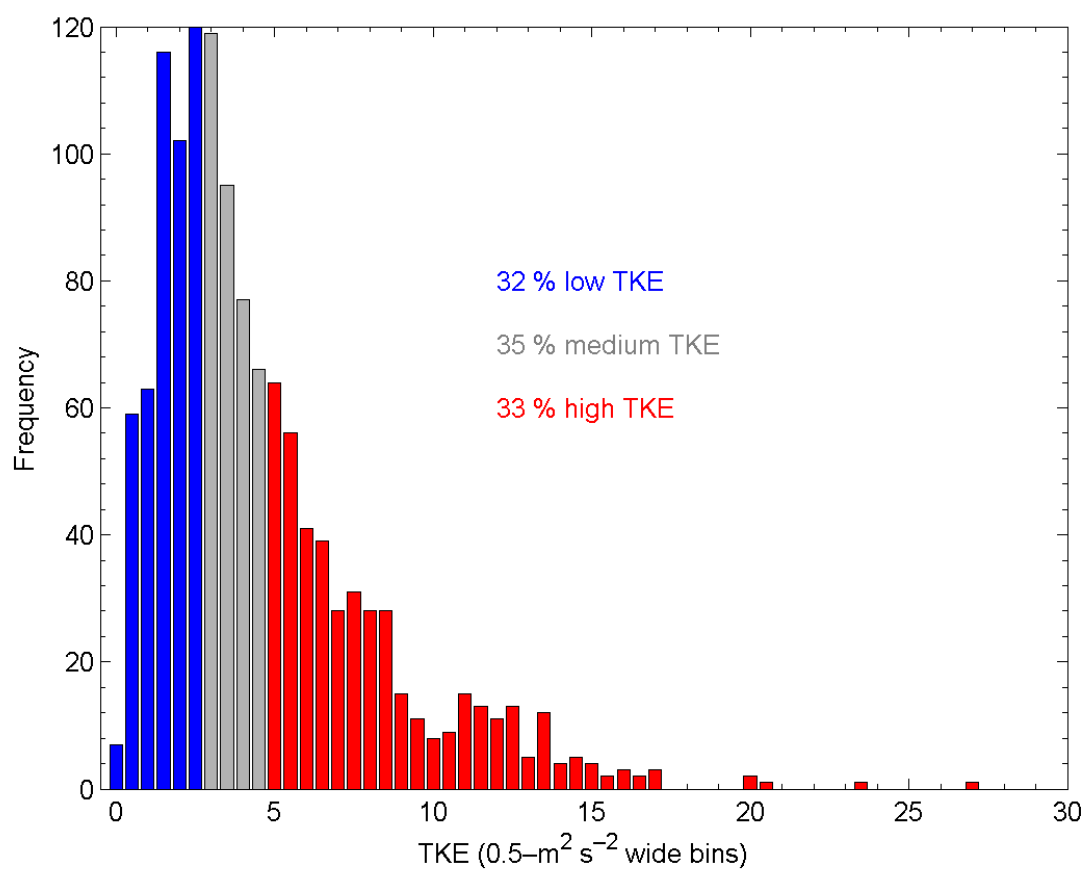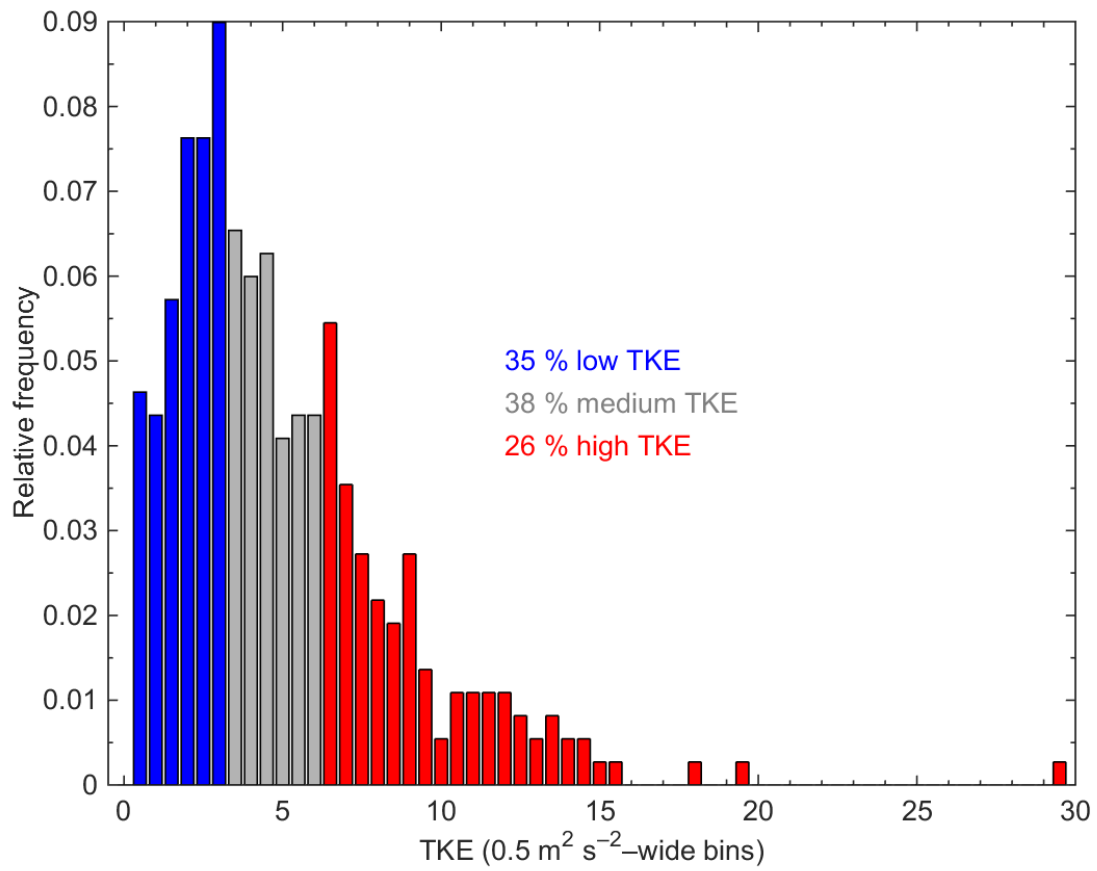
Figure ~~14~~15. TKE distribution using thresholds in Table 3. Includes data filtered for tower 80‑m wind speeds between 3.5 and

25.0 m s^{-1}, 87‑m wind directions between 235° and 315°, and for normal turbine operation ~~blade pitch angle within ± 3 MAD~~.
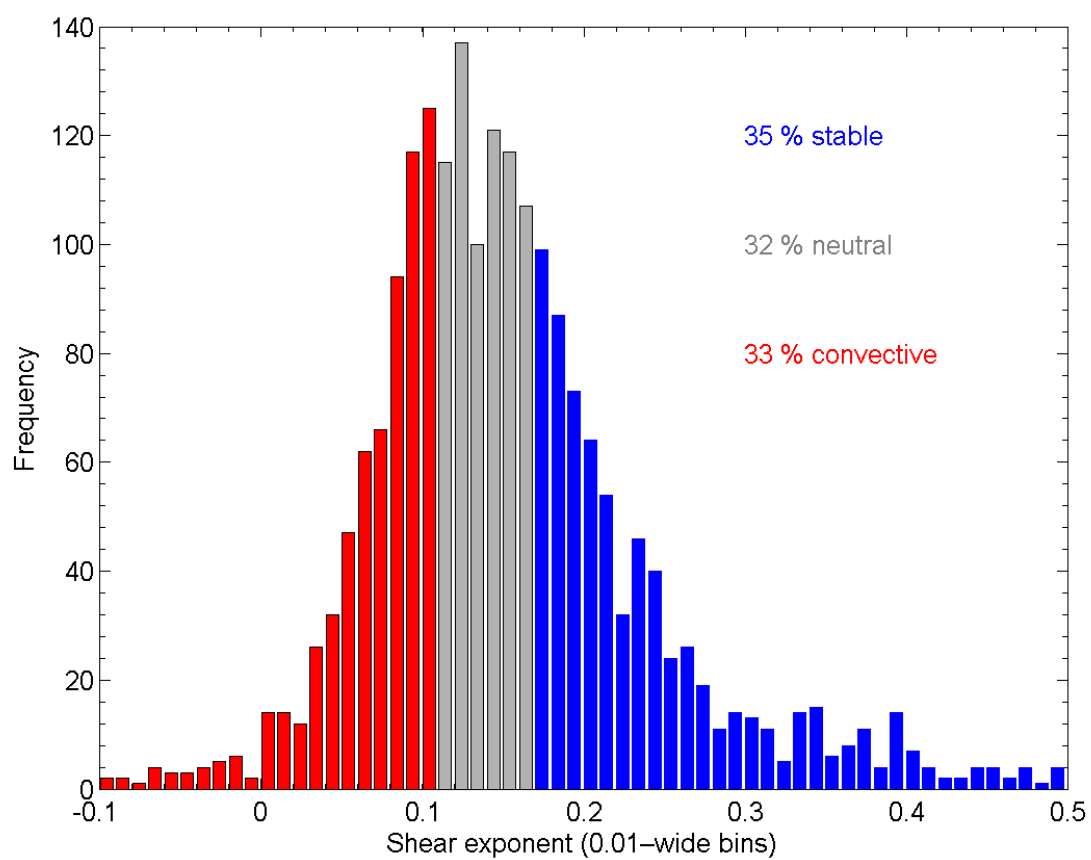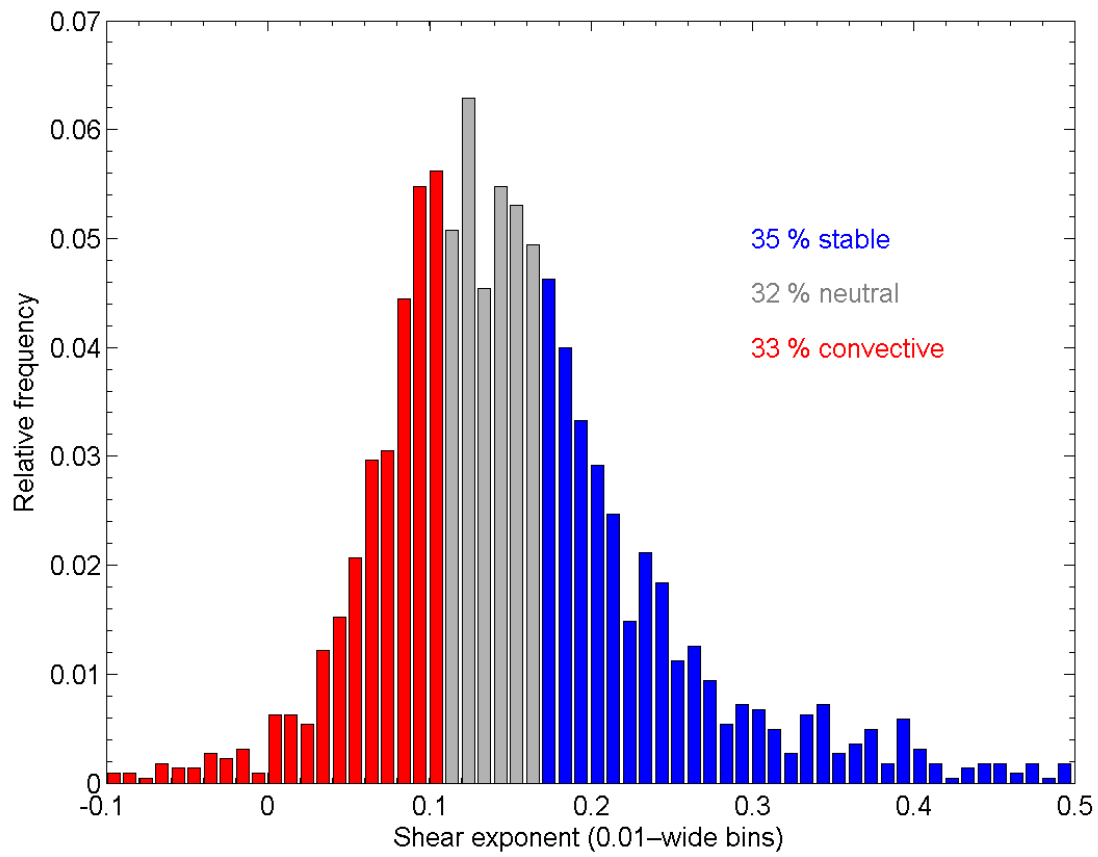
Figure ~~15~~16. Shear exponent distribution using thresholds in Table 2. Includes data filtered for tower 80‐m wind speeds between

3.5 and 25.0 m s^{-1}, 87‐m wind directions between 235° and 315°, and~~for normal turbine operation~~ blade pitch angle within ± 3

~~MAD~~.
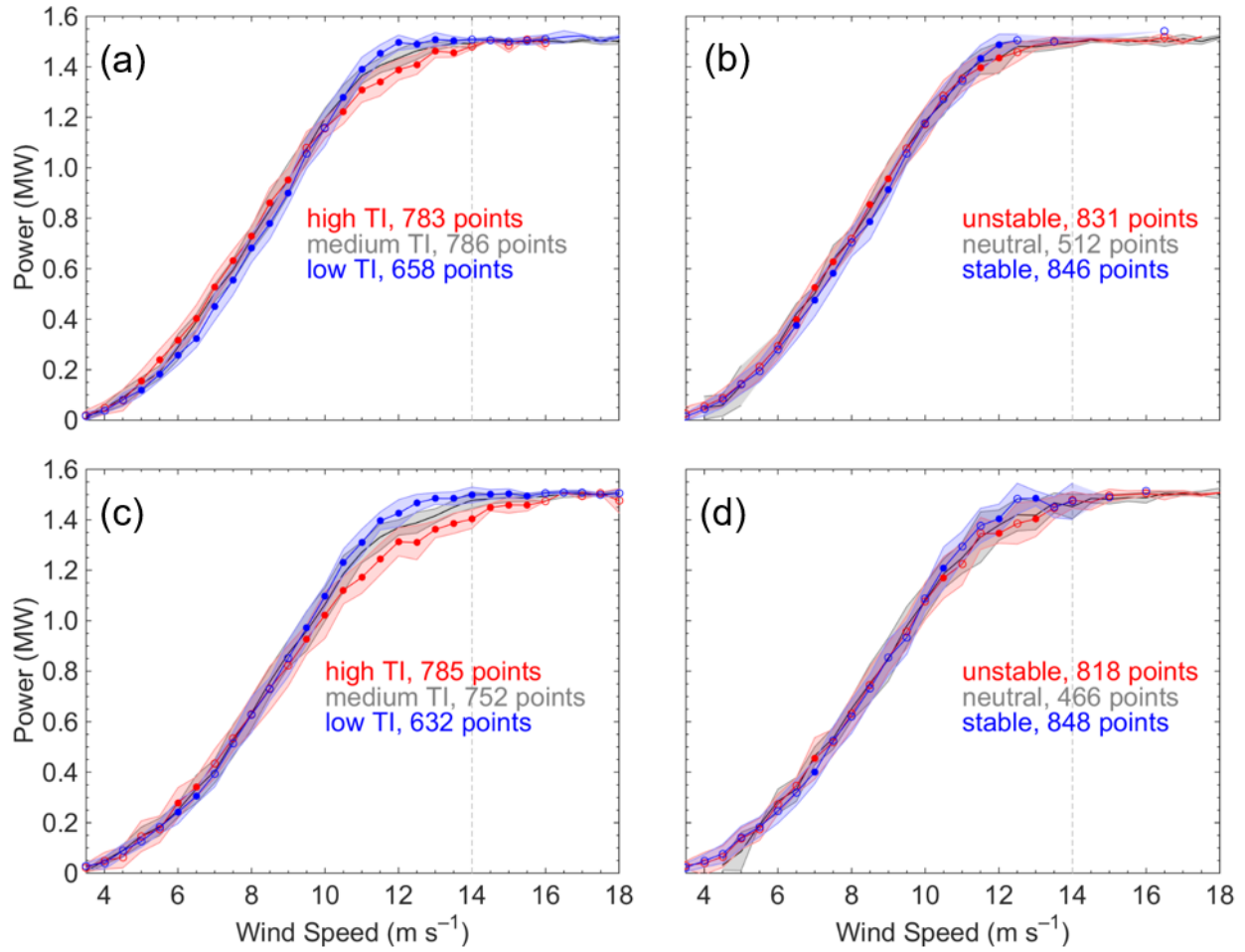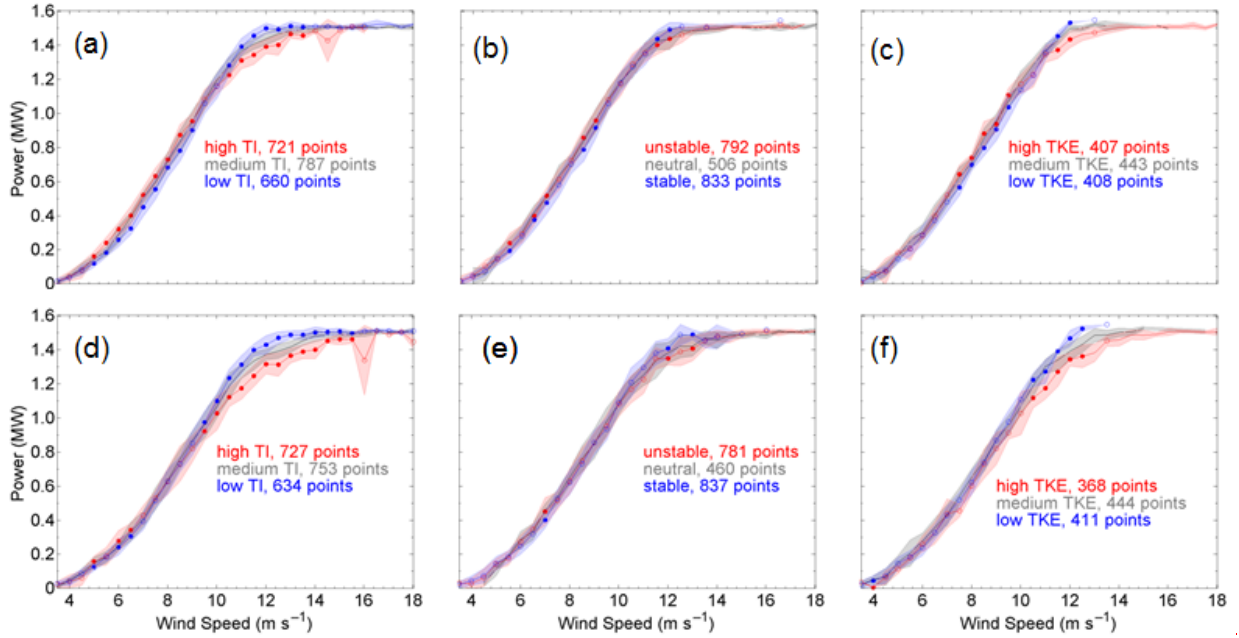
Figure 17. Nacelle anemometer power curves with (a) TI regimes and (b) R_B regimes. Eighty-meter tower anemometer power curves with (c) TI regimes and (d) R_B regimes. Median statistics are used to avoid outlier effects. Statistically distinct differences within each wind speed bin between the regimes are determined by the Wilcoxon rank sum test with a 1 % significance level and denoted by closed circles. Includes data filtered for tower 80-m wind speeds between 3.5 and 25.0 m s^{-1}, 87-m wind directions between 235° and 315°, and for normal turbine operation. Envelopes represent ± 1 MAD for each wind speed bin. The grey dashed line marks rated speed.

Figure 17~~18~~. Nacelle anemometer power curves shown as the anomaly from the neutral or medium power curve of the (a) TI regimes ~~and;~~ (b) R_B regimes~~; and (c) TKE regimes~~. Eighty-meter tower anemometer power curves shown as the anomaly from the neutral or medium power curve of the (c~~d~~) TI regimes ~~and;~~ (d~~e~~) R_B regimes~~; and (f) TKE regimes~~. Median statistics are used to avoid outlier effects. Statistically distinct differences within each wind speed bin between the regimes are determined by the Wilcoxon rank sum test with a 1 % significance level and denoted by closed circles. Includes data filtered for tower 80-m wind speeds between 3.5 and 25.0 m s^{-1}, 87-m wind directions between 235° and 315°, ~~and~~ and for normal turbine operation ~~blade pitch angle within ± 3 MAD~~. Envelopes represent ± 1 MAD for each wind speed bin. The grey dashed line marks rated speed.